

Recent Advances in 3D Gaussian Splatting

Tong Wu¹, Yu-Jie Yuan¹, Ling-Xiao Zhang¹, Jie Yang¹, Yan-Pei Cao², Ling-Qi Yan³, and Lin Gao¹(✉)

© The Author(s)

Abstract The emergence of 3D Gaussian Splatting (3DGS) has greatly accelerated the rendering speed of novel view synthesis. Unlike neural implicit representations like Neural Radiance Fields (NeRF) that represent a 3D scene with position and viewpoint-conditioned neural networks, 3D Gaussian Splatting utilizes a set of Gaussian ellipsoids to model the scene so that efficient rendering can be accomplished by rasterizing Gaussian ellipsoids into images. Apart from the fast rendering speed, the explicit representation of 3D Gaussian Splatting facilitates editing tasks like dynamic reconstruction, geometry editing, and physical simulation. Considering the rapid change and growing number of works in this field, we present a literature review of recent 3D Gaussian Splatting methods, which can be roughly classified into 3D reconstruction, 3D editing, and other downstream applications by functionality. Traditional point-based rendering methods and the rendering formulation of 3D Gaussian Splatting are also illustrated for a better understanding of this technique. This survey aims to help beginners get into this field quickly and provide experience researchers with a comprehensive overview, which can stimulate the future development of the 3D Gaussian Splatting representation.

Keywords 3D Gaussian Splatting, radiance field, novel view synthesis, editing, generation

1 Introduction

With the development of virtual reality and augmented reality, the demand for realistic 3D content is increasing. Tradi-

tional 3D content creation methods include 3D reconstruction from scanners or multi-view images and 3D modeling with professional software. However, traditional 3D reconstruction methods are likely to produce less faithful results due to imperfect capture and noisy camera estimation. 3D modeling methods yield realistic 3D content but require professional user training and interaction, which is time-consuming.

To create realistic 3D content automatically, Neural radiance fields (NeRF) [1] propose to model a 3D scene's geometry and appearance with a density field and a color field, respectively. NeRF greatly improved the quality of novel view synthesis results but still suffered from its low training and rendering speed. While significant efforts [2–4] have been made to accelerate it to facilitate its applications on common devices, it is still hard to find a robust method that can both train a NeRF quickly enough (≤ 1 hour) on a consumer-level GPU and render a 3D scene at an interactive frame rate (~ 30 FPS) on common devices like cellphones and laptops. To resolve the speed issues, 3D Gaussian Splatting (3DGS) [5] proposes to rasterize a set of Gaussian ellipsoids to approximate the appearance of a 3D scene, which not only achieves comparable novel view synthesis quality but also allows fast converge (~ 30 minutes) and real-time rendering (≥ 30 FPS) at 1080p resolution, making low-cost 3D content creation and real-time applications possible.

Based on the 3D Gaussian Splatting representation, a number of research works have come out and more are on the way. To help readers get familiar with 3D Gaussian Splatting quickly, we present a survey on 3D Gaussian Splatting, which covers both traditional splatting methods and recent neural-based 3DGS methods. As shown in Fig. 1, we divide these works into three parts by functionality. We first introduce how 3D Gaussian Splatting allows realistic scene reconstruction under various sceneries (Sec. 2) and further present scene editing techniques with 3D Gaussian Splatting (Sec. 3) and how 3D Gaussian Splatting makes downstream applications like digital human possible (Sec. 4). Finally, we

1 Institute of Computing Technology, Chinese Academy of Sciences, Beijing, China, 100190. E-mail: Tong Wu, wutong19s@ict.ac.cn; Yu-Jie Yuan, yuanyujie@ict.ac.cn; Ling-Xiao Zhang, zhanglingxiao@ict.ac.cn; Jie Yang, yangjie01@ict.ac.cn; Lin Gao, gaolin@ict.ac.cn.

2 VAST. Yan-Pei Cao, caoyanpei@gmail.com.

3 Department of Computer Science, University of California. Ling-Qi Yan, lingqi@cs.ucsb.edu.

Manuscript received: 2024-02-28;

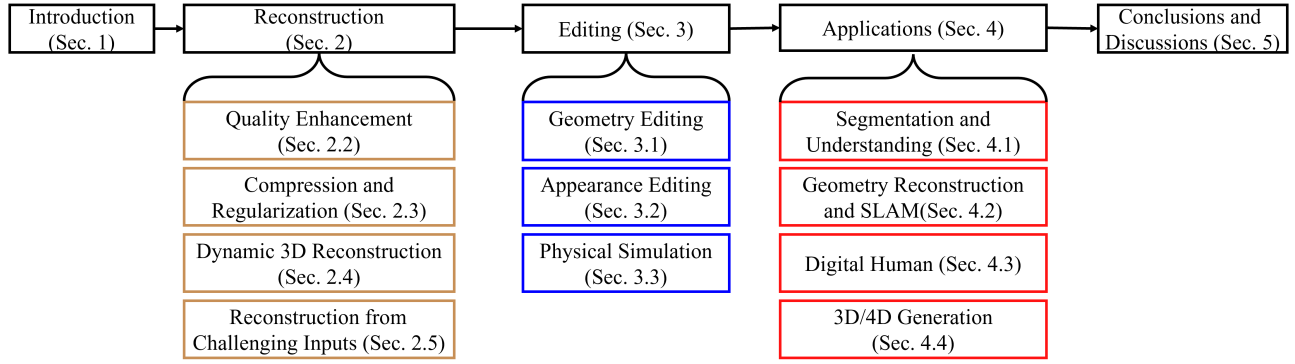


Fig. 1 Structure of the literature review and taxonomy of current 3D Gaussian Splatting methods.

summarize recent research works on 3D Gaussian Splatting at a higher level and present future works remaining to be done in this field (Sec. 5). A timeline of representative works can be found in Fig. 2.

2 Gaussian Splatting for 3D Reconstruction

2.1 Point-based Rendering

Point-based rendering technique aims to generate realistic images by rendering a set of discrete geometry primitives. Grossman and Dally [6] propose the point-based rendering technique based on the purely point-based representation, where each point only influences one pixel on the screen. Instead of rendering points, Zwicker *et al.* [7] propose to render splats (ellipsoids) so that each splat can occupy multiple pixels and the mutual overlap between them can generate hole-free images more easily than purely point-based representation. Later, a series of splatting methods aim to enhance it by introducing a texture filter for anti-aliasing rendering [8], improving rendering efficiency [9, 10], and resolving discontinuous shading [11]. For more details about traditional point-based rendering techniques, please refer to [12].

Traditional point-based rendering methods focus more on how to produce high-quality rendered results with a given geometry. With the development of recent implicit representation [13–15], researchers have started to explore point-based rendering with the neural implicit representation without any given geometry for the 3D reconstruction task. One representative work is NeRF [1] which models geometry with an implicit density field and predicts view-dependent color c_i with another appearance field. The point-based rendering combines all sample points' color on a camera ray to produce a pixel color C by:

$$C = \sum_{i=1}^N c_i \alpha_i T_i \quad (1)$$

where N is the number of sample points on a ray and $\alpha_i = \exp(-\sum_{j=1}^{i-1} \sigma_j \delta_j)$ are the view-dependent color and

the opacity value for i th point on the ray. σ_j is the j th point's density value. $T_i = \prod_{j=1}^{i-1} (1 - \alpha_j)$ is accumulated transmittance. To ensure high-quality rendering, NeRF [1] typically requires sampling 128 points on a single ray, which unavoidably takes longer time to train and render.

To speed up both training and rendering, instead of predicting density values and colors for all sample points with neural networks, 3D Gaussian Splatting [5] abandons the neural network and directly optimizes Gaussian ellipsoids to which attributes like position P , rotation R , scale S , opacity α and Spherical Harmonic coefficients (SH) representing view-dependent color are attached. The pixel color is determined by Gaussian ellipsoids projected onto it from a given viewpoint. The projection of 3D Gaussian ellipsoids can be formulated as:

$$\Sigma' = JW\Sigma W^T J^T \quad (2)$$

where Σ' and $\Sigma = RSS^T R^T$ are the covariance matrices for 3D Gaussian ellipsoids and projected Gaussian ellipsoids on 2D image from a viewpoint with viewing transformation matrix W . J is the Jacobian matrix for the projective transformation. 3DGS shares a similar rendering process with NeRF but there are two major differences between them:

- (1) 3DGS models opacity values directly while NeRF transforms density values to the opacity values.
- (2) 3DGS uses rasterization-based rendering which does not require sampling points while NeRF requires dense sampling in the 3D space.

Without sampling points and querying the neural network, 3DGS becomes extremely fast and achieves ~ 30 FPS on a common device with comparable rendering quality with NeRF.

2.2 Quality Enhancement

Though producing high-quality reconstruction results, there are still improvement spaces for 3DGS's rendering. Mip-

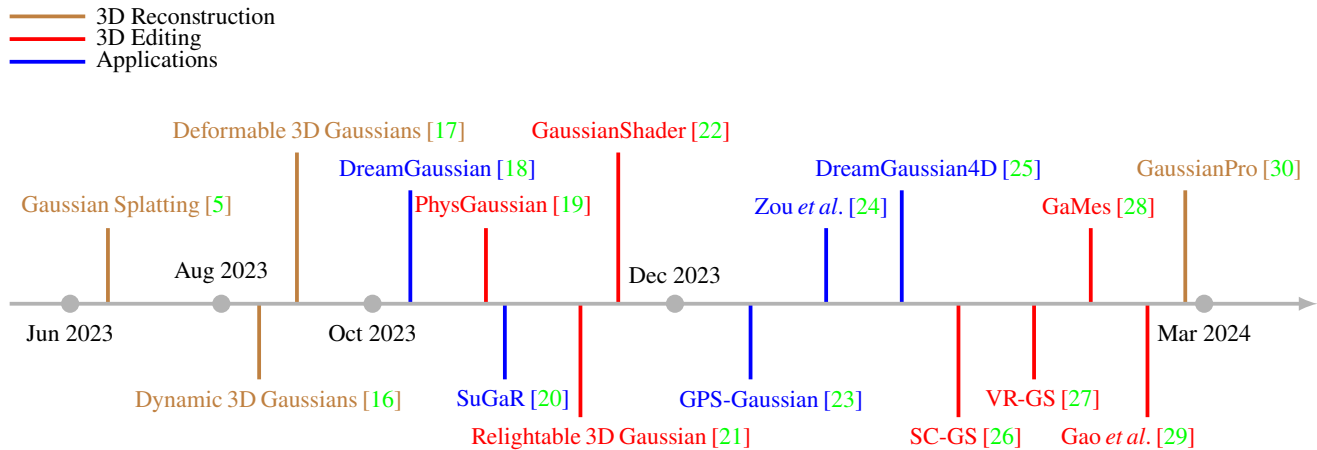


Fig. 2 A brief timeline of representative works with the 3D Gaussian Splatting representation.

Splatting [31] observed that changing the sampling rate, for example, the focal length, can greatly influence the quality of rendered images by introducing high-frequency Gaussian shape-like artifacts or strong dilation effects. To eliminate the high-frequency Gaussian shape-like artifacts, Mip-Splatting [31] constrains the frequency of the 3D representation to be below half the maximum sampling frequency determined by the training images. In addition, to avoid the dilation effects, it introduces another 2D Mip filter to projected Gaussian ellipsoids to approximate the box filter similar to EWA-Splatting [8]. MS3DGS [32] also aims at solving the aliasing problem in the original 3DGS and introduces a multi-scale Gaussian splatting representation and when rendering a scene at a novel resolution level, it selects Gaussians from different scale levels to produce alias-free images.

Apart from the aliasing problem, the capability of rendering view-dependent effects also needs to be improved. To produce more faithful view-dependent effects, VDGS [33] proposes to model the 3DGS to represent 3D shapes and predict attributes like view-dependent color and opacity with NeRF-like neural network instead of Spherical Harmonic (SH) coefficients in the original 3DGS. Scaffold-GS [34] proposes to initialize a voxel grid and attach learnable features onto each voxel point and all attributes of Gaussians are determined by interpolated features and lightweight neural networks. Instead of changing the view-dependent appearance modeling approach, StopThePop [35] points out that 3DGS tends to cheat view-dependent effects by popping 3D Gaussians due to the per-ray depth sorting, which leads to less faithful results when the viewpoint is rotated. To mitigate the potential of popping 3D Gaussians, StopThePop [35] replaces the per-ray depth sorting with tile-based sorting to ensure consistent sorting order at a local region.

Table 1 Quantitative comparison of novel view synthesis results on the MipNeRF 360 dataset [37] using PSNR, SSIM and LPIPS metrics.

Methods	PSNR \uparrow	SSIM \uparrow	LPIPS \downarrow
MipNeRF [38]	24.04	0.616	0.441
MipNeRF 360 [37]	27.57	0.793	0.234
ZipNeRF [39]	28.54	0.828	0.189
3DGS [5]	27.21	0.815	0.214
Mip-Splatting [31]	27.79	0.827	0.203
Scaffold-GS [34]	28.84	0.848	0.220
VDGS [33]	27.66	0.809	0.223
GaussianPro [30]	27.92	0.825	0.208

To better guide the growth of 3D Gaussian Splatting, GaussianPro [30] introduces a progressive propagation strategy to updating Gaussians by considering the normal consistency between neighboring views and adding plane constraints as shown in Fig. 3. To deal with more complex shadings like specular and anisotropic components, Spec-Gaussian [36] proposes to utilize Anisotropic Spherical Gaussian to approximate 3D scenes' appearance. Quantitative results of different reconstruction methods can be found in Table 1. 3DGS-based methods and NeRF-based methods are comparable but 3DGS-based methods have faster rendering speed.

2.3 Compression and Regularization

Although the 3D Gaussian Splatting achieves real-time rendering, there is improvement space in terms of lower computational requirements and better point distribution. Some methods focus on changing the original representation to reduce computational resources.

Vector Quantization, a traditional compression method in signal processing, which involves clustering multi-dimensional data into a finite set of representations, is mainly utilized in Gaussians [40–44]. C3DGS [40] adopts residual

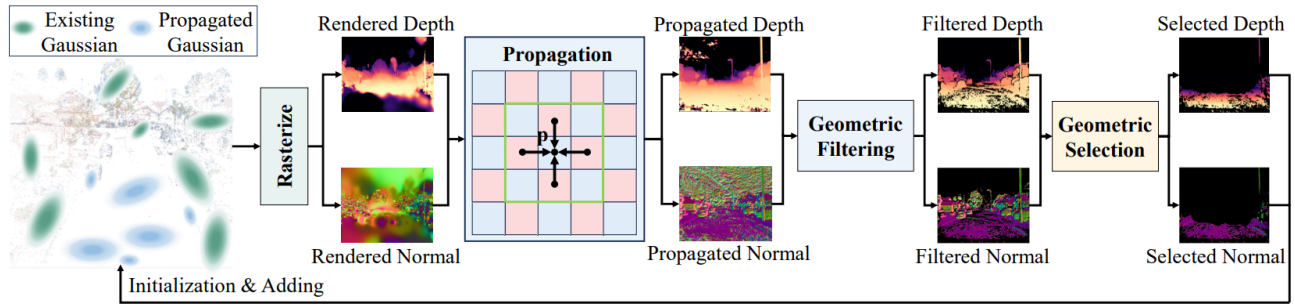


Fig. 3 Overview of GaussianPro [30]. Neighboring views' normal direction consistency is considered to produce better reconstruction results.

Table 2 Comparison of different compression methods on the MipNeRF360 [37] dataset. Size is measured in MB.

Methods	SSIM \uparrow	PSNR \uparrow	LPIPS \downarrow	Size \downarrow
3DGS[5]	0.815	27.21	0.214	750
C3DGS[40]	0.798	27.08	0.247	48.8
Compact3D [41]	0.808	27.16	0.228	/
EAGLES [43]	0.81	27.15	0.24	68
SOGS[47]	0.763	25.83	0.273	18.2
SASCGS[42]	0.801	26.98	0.238	28.80
LightGaussian [44]	0.857	28.45	0.210	42.48

vector quantization (R-VQ) [45] to represent geometric attributes, including scaling and rotation. SASCGS [42] utilizes vector clustering to encode color and geometric attributes into two codebooks, with a sensitivity-aware K-Means method. As shown in Fig. 4, EAGLES [43] quantizes all attributes including color, position, opacity, rotation, and scaling, they show that the quantization of opacity leads to fewer floaters or visual artifacts in the novel view synthesis task. Compact3D [41] does not quantize opacity and position, because sharing them results in overlapping Gaussians. LightGaussian [44] adopts octree-based lossless compression in G-PCC [46] for the position attribute due to the sensitivity to the subsequent rasterization accuracy for the position. SOGS [47] adopt a different method from Vector Quantization. They arrange Gaussian attributes into multiple 2D grids. These grids are sorted and a smoothness regularization is applied to penalize all pixels that have very different values compared to their local neighborhood on the 2D grid.

In terms of disk data storage, SASCGS [42] utilizes the entropy encoding method DEFLATE, which utilizes a combination of the LZ77 algorithm and Huffman coding, to compress the data. SOGS [47] compress the RGB grid with JPEG XL and store all other attributes as 32-bit OpenEXR images with zip compression. Quantitative reconstruction results and sizes of 3D scenes after compression are shown in Table 2.

2.4 Dynamic 3D Reconstruction

The same as the NeRF representation, 3DGS can also be extended to reconstruct dynamic scenes. The core of dynamic 3DGS lies in how to model the variations of Gaussian attribute values over time. The most straightforward way is to assign different attribute values to 3D Gaussian at different timesteps. Luiten *et al.* [16] regard the center and rotation (quaternion) of 3D Gaussian as variables that change over time, while other attributes remain constant over all timesteps, thus achieving 6-DOF tracking by reconstructing dynamic scenes. However, the frame-by-frame discrete definition lacks continuity, which can cause poor results in long-term tracking. Therefore, physical-based constraints are introduced, which are three regularization losses, including short-term local-rigidity and local-rotation similarity losses and a long-term local-isometry loss. However, this method still lacks inter-frame correlation and requires high storage overhead for long-term sequences. Therefore, decomposing spatial and temporal information and modeling them with a canonical space and a deformation field, respectively, has become another exploration direction. The canonical space is the static 3DGS, then the problem becomes how to model the deformation field. One way is to use an MLP network to implicitly fit it, similar to the dynamic NeRF [48]. Yang *et al.* [17] follow this idea and propose to input the positional-encoded Gaussian position and timestep t to the MLP which outputs the offsets of the position, rotation, and scaling of 3D Gaussian. However, inaccurate poses may affect rendering quality. This is not significant in continuous modeling of NeRF, but discrete 3DGS can amplify this problem, especially in the time interpolation task. So, they add a linearly decaying Gaussian noise to the encoded time vector to improve temporal smoothing without additional computational overhead. Some results are shown in Fig. 5. 4D-GS [49] adopts the multi-resolution HexPlane voxels [50] to encode the temporal and spatial information of each 3D Gaussian

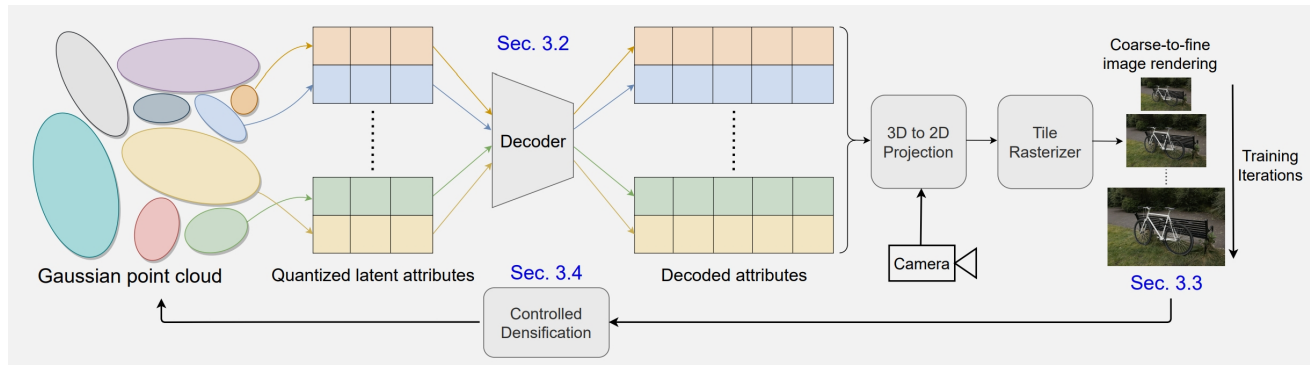


Fig. 4 Pipeline from EAGLES [43]. Vector Quantization (VQ) is utilized to compress Gaussian attributes.

rather than positional encoding and utilizes different compact MLPs for different attributes. For stable training, it first optimizes static 3DGS and then optimizes the deformation field represented by an MLP. GauFRe [51] applies the exponential and normalization operation to the scaling and rotation respectively after adding the delta values predicted by an MLP, ensuring convenient and reasonable optimization. As dynamic scenes contain large static parts, it randomly initializes the point cloud into dynamic point clouds and static point clouds, optimizes them accordingly, and renders them together to achieve decoupling of the dynamic part and the static part.

Compared to NeRF, 3DGS is an explicit representation and the implicit deformation modeling requires lots of parameters which may bring overfit, so some explicit deformation modeling methods are also proposed, which ensure fast training. Katsumata *et al.* [52] propose to use the Fourier series to fit the changes of the Gaussian position, inspired by the fact that the motion of human and articulated objects is sometimes periodic. The rotation is approximated by a linear function. Other attributes remain unchanged over time. So dynamic optimization is to optimize the parameters of the Fourier series and the linear function, and the number of parameters is independent of time. These parametric functions are continuous functions about time, ensuring temporal continuity and thus ensuring the robustness of novel view synthesis. In addition to the image losses, a bidirectional optical flow loss is also introduced. The polynomial fitting and Fourier approximation have advantages in modeling smooth motion and violent motion, respectively. So Gaussian-Flow [53] combines these two methods in the time and frequency domains to capture the time-dependent residuals of the attribute, named as Dual-Domain Deformation Model (DDDM). The position, rotation, and color are considered to change over time. To prevent optimization problems caused by uniform time division, this work adopts adaptive timestep scaling. Finally, the op-

Table 3 Quantitative comparison of novel view synthesis results on the D-NeRF [48] dataset using PSNR, SSIM and LPIPS metrics.

Methods	PSNR \uparrow	SSIM \uparrow	LPIPS \downarrow
D-NeRF [48]	31.69	0.975	0.057
TiNeuVox [57]	33.76	0.984	0.044
Tensor4D [58]	27.72	0.945	0.051
K-Planes [59]	32.32	0.973	0.038
CoGS [60]	37.90	0.983	0.027
GauFRe [51]	34.80	0.985	0.028
4D-GS [49]	34.01	0.989	0.025
Yang <i>et al.</i> [17]	39.51	0.990	0.012

timization iterates between static optimization and dynamic optimization, and introduces temporal smoothness loss and KNN rigid loss. Li *et al.* [54] introduce a temporal radial basis function to represent temporal opacity, which can effectively model the scene content that emerges or vanishes. Then, the polynomial function is exploited to model the motion and rotation of 3D Gaussians. They also replace the spherical harmonics with features to represent view- and time-related color. These features consist of three parts: base color, view-related feature, and time-related feature. The latter two are translated into a residual color through an MLP added to the base color to obtain the final color. During optimization, new 3D Gaussians will be sampled at the under-optimized positions based on training error and coarse depth. The explicit modeling methods used in the above methods are all based on commonly used functions. DynMF [55] assumes that each dynamic scene is composed of a finite and fixed number of motion trajectories and argues that a learned basis of the trajectories will be smoother and more expressive. All motion trajectories in the scene can be linearly represented by this learned basis and a small temporal MLP is used to generate the basis. The position and rotation change over time and both share the motion coefficients with different motion bases. The regularization, sparsity, and local rigidity terms of the motion coefficients are introduced during optimization.

There are also some other ways to explore. 4DGS [61] re-

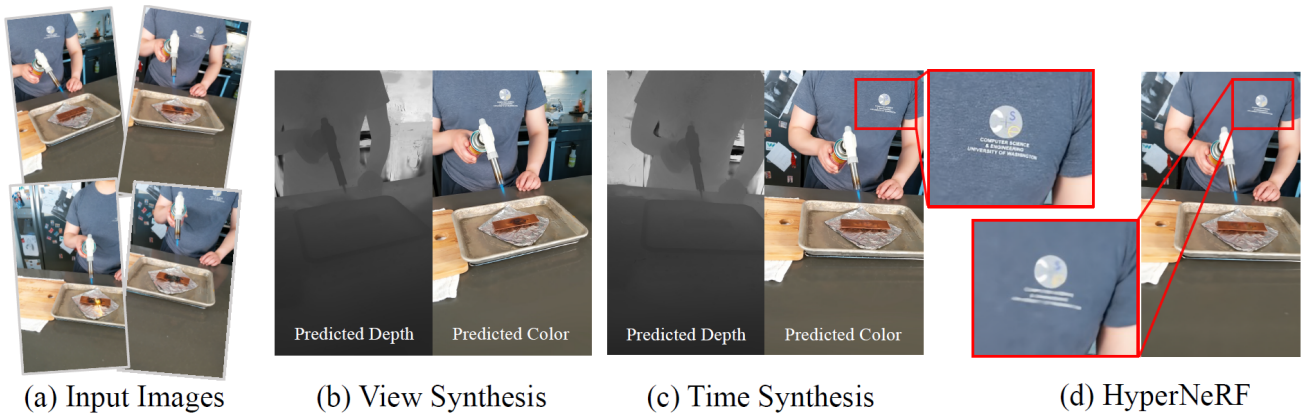


Fig. 5 The results of Deformable3DGS [17]. Given a set of monocular multi-view images (a), this method can achieve novel view synthesis (b) and time synthesis (c), and has better rendering quality compared to HyperNeRF [56] (d).

gards the spacetime of the scene as an entirety and transforms 3D Gaussian into 4D Gaussian, that is, transforming the attribute values defined on Gaussian to 4D space. For example, the scaling matrix is diagonal, so adding a scaling factor of time dimension on the diagonal forms the scaling matrix in 4D space. The 4D extension of the spherical harmonics (SH) can be expressed as the combination of SH with 1D-basis functions. SWAGS [62] divides the dynamic sequence into different windows based on the amount of motion and trains separate dynamic 3DGS model in different windows, with different canonical spaces and deformation fields. The deformation field uses a tunable MLP [63], which focuses more on modeling the dynamic part of the scene. Finally, fine-tuning ensures temporal consistency between windows using the overlapping frame to add constraints. The MLP is fixed and only the canonical representation is optimized during fine-tuning.

These dynamic modeling methods can be further applied in the medical field, such as the markless motion reconstruction for motion analysis of infants and neonates [64] which introduces additional mask and depth supervisions, and monocular endoscopic reconstruction [65, 66]. Quantitative reconstruction results by representative NeRF-based and 3DGS-based methods are reported in Table 3. 3DGS-based methods have clear advantages compared to NeRF-based methods due to their explicit geometry representation that can model the dynamics more easily.

2.5 3D Reconstruction from Challenging Inputs

While most methods experiment on regular input data with dense viewpoints in relatively small scenes, there are also works targeting reconstructing 3D scenes with challenging inputs like sparse-view input, data without camera parameters, and larger scenes like urban streets. FSGS [67] is the

first to explore reconstructing 3D scenes from sparse view input. It initializes sparse Gaussians from structure-from-motion (SfM) methods and identifies them by unpooling existing Gaussians. To allow faithful geometry reconstruction, an extra pre-trained 2D depth estimation network helps to supervise the rendered depth images. SparseGS [68] also targets 3D reconstruction from sparse-view inputs by introducing depth inputs estimated by pre-trained a 2D network. It further removes Gaussians with incorrect depth values and utilizes the Score Distillation Sampling (SDS) loss [69] to encourage rendered results from novel viewpoints to be more faithful. GaussainObject [70] instead initializes Gaussians with visual hull and fine-tunes a pre-trained ControlNet [71] repair degraded rendered images generated by adding noises to Gaussians' attributes, which outperforms previous NeRF-based sparse-view reconstruction methods as shown in Fig. 6.

Moving a step forward, pixelSplat [72] reconstructs 3D scenes from single-view input without any data priors. It extracts pixel-aligned image features similar to PixelNeRF [73] and predicts attributes for each Gaussian with neural networks. SplatterImage [74] also works on single-view data but instead utilizes a U-Net [75] network to translate the input image into attributes on Gaussians. It can extend to multi-view inputs by aggregating predicted Gaussians from different viewpoints via warping operation.

For urban scene data, PVG [78] makes Gaussian's mean and opacity value time-dependent functions centered at corresponding Gaussian's life peak (maximum prominence over time). DrivingGaussian [79] reconstructs dynamic driving data by first incrementally optimizing static 3D Gaussians and then composing them with dynamic objects' 3D Gaussians. This process is also assisted by the Segmentation Anything Model [80] and input LiDAR depth data. StreetGaussians [81] models the static background with a static 3DGS

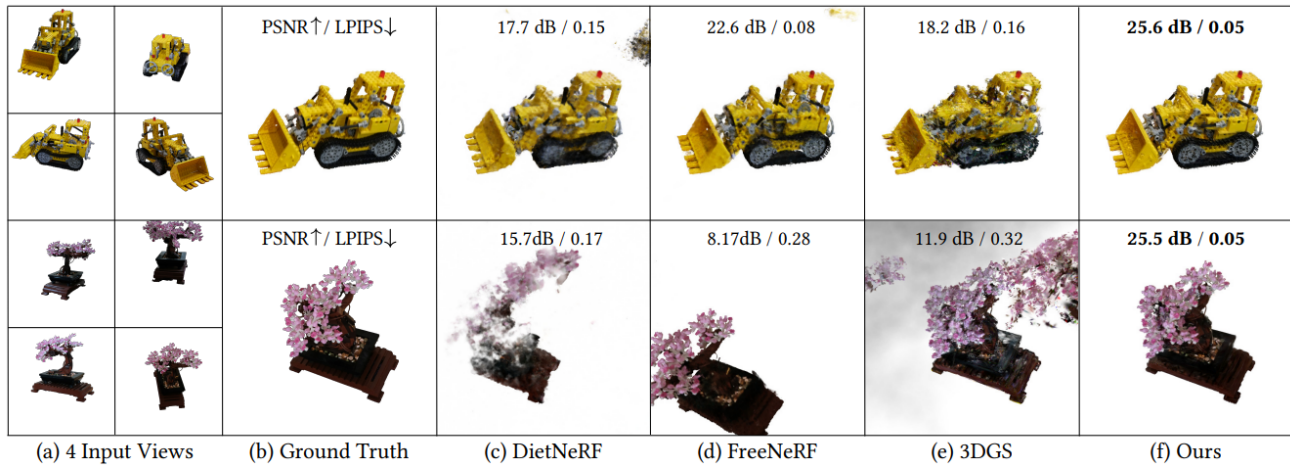


Fig. 6 Results by GaussianObject [70]. Compared to previous NeRF-based sparse-view reconstruction methods [76, 77] and recent 3DGS [5], GaussianObject achieves high-quality 3D reconstruction from only 4 views.

and dynamic objects by a dynamic 3DGS where Gaussians are transformed by tracked vehicle poses and their appearance is approximated with time-related Spherical Harmonics (SH) coefficients. To facilitate comparisons on the urban scenes for 3DGS methods, GauU-Scene [82] provides a large-scale dataset covering over $1.5km^2$.

Apart from the works mentioned above, other methods focus on special input data including images without camera [83, 84], blurry inputs [85], CT scans [86], panoramic images [87], and satellite images [88].

3 Gaussian Splatting for 3D Editing

3DGS allows for efficient training and high-quality real-time rendering using rasterization-based point-based rendering techniques. Editing in 3DGS has been investigated in a number of fields. We have summarized the editing on 3DGS into three categories: geometry editing, appearance editing, and physical simulation.

3.1 Geometry Editing

On the geometry side, GaussianEditor [89] controls the 3DGS using the text prompts and semantic information from proposed Gaussian semantic tracing, which enables 3D inpainting, object removal, and composition for Gaussian Splatting. Gaussian Grouping [90] simultaneously rebuilds and segments open-world 3D objects under the supervision of 2D mask predictions from SAM and 3D spatial consistency constraints, which further enables diverse editing applications including 3D object removal, inpainting, and composition with high-quality visual effects and time efficiency. Furthermore, Point'n Move [91] combines interactive scene object manipulation with exposed region inpainting. Thanks

to the explicit representation of 3DGS, the dual-stage self-prompting mask propagation process is proposed to transfer the given 2D prompt points to 3D mask segmentation, resulting in a user-friendly editing experience with high-quality effects. Although the above methods realize the editing on 3DGS, they are still limited to some simple editing operations (removal, rotation, and translation) for 3D objects. SuGaR [20] extracts explicit meshes from the 3DGS representation by regularizing Gaussians over surfaces. Further, it relies on manual adjustment of Gaussian parameters based on deformed meshes to realize desired geometry editing but struggles with large-scale deformation. SC-GS [26] learns a set of sparse control points for 3D scene dynamics but faces challenges with intense movements and detailed surface deformation. GaMeS [28] introduces a new GS-based model that combines conventional mesh and vanilla GS. The explicit mesh is utilized as input and parameterizes Gaussian components using the vertices, which can modify Gaussians in real time by altering mesh components during inference. However, it cannot handle significant deformations or changes, especially the deformation on large faces, since it cannot change the mesh topology during training. Although the above methods can finish some simple rigid transformations and non-rigid deformation, they still face challenges in their editing effectiveness and large-scale deformation. As shown in Fig. 7, Gao *et al.* [29] also adapt the mesh-based deformation to 3DGS by harnessing the priors of explicit representation (the surface properties like normals of the mesh, and the gradients generated by explicit deformation methods) and learning the face split to optimize the parameters and number of Gaussians, which provides adequate topological information to 3DGS and improves the quality for both

the reconstruction and geometry editing results.

3.2 Appearance Editing

On the appearance side, GaussianEditor [92] proposes to first modify 2D images with language input with diffusion model [93] in the masked region generated by the recent 2D segmentation model [80] and updating attributes of Gaussians again similar to the previous NeRF editing work Instruct-NeRF2NeRF [94]. Another independent research work also named GaussianEditor [89] operates similarly but it further introduces a Hierarchical Gaussian Splatting (HGS) to allow 3D editing like object inpainting.

To allow more tractable control over texture and lighting, researchers have started to disentangle texture and lighting to enable independent editing. As shown in Fig. 8, GS-IR [95] and RelightableGaussian [21] separately model texture and lighting. Additional materials parameters are defined on each Gaussian to represent texture and lighting is approximated by a learnable environment map. GIR [96] and Gaussian-Shader [22] share the same disentanglement paradigm by binding material parameters onto 3D Gaussians, but to deal with more challenging reflective scenes, they add normal orientation constraints to Gaussians similar to Ref-NeRF [97]. After texture and lighting disentanglement, these methods can independently modify texture or lighting without influencing the other.

3.3 Physical Simulation

On the physical-based 3DGS editing, as shown in Fig. 9, PhysGaussian [19] employs discrete particle clouds from 3D GS for physically-based dynamics and photo-realistic rendering through continuum deformation [98] of Gaussian kernels. Gaussian Splashing [99] combines 3DGS and position-based dynamics (PBD) [100] to manage rendering, view synthesis, and solid/fluid dynamics cohesively. Similar to Gaussian shaders [22], the normal is applied to each Gaussian kernel to align its orientation with the surface normal and improve PBD simulation, also allowing the physically-based rendering to enhance dynamic surface reflections on fluids. VR-GS [27] is a physical dynamics-aware interactive Gaussian Splatting system for VR, tackling the difficulty of editing high-fidelity virtual content in real time. VR-GS utilizes 3DGS to close the quality gap between generated and manually crafted 3D content. By utilizing physically-based dynamics, which enhance immersion and offer precise interaction and manipulation controllability.

4 Applications of Gaussian Splatting

4.1 Segmentation and Understanding

Open-world 3D scene understanding is an essential challenge for robotics, autonomous driving, and VR/AR environments. With the remarkable progress in 2D scene understanding brought by SAM [80] and its variants, existing methods have tried to integrate semantic features, such as CLIP [101]/DINO [102] into NeRF, to deal with 3D segmentation, understanding, and editing.

NeRF-based methods are computationally intensive because of the implicit and continuous representation. Recent methods try to integrate 2D scene understanding methods with 3D Gaussians to produce a real-time and easy-to-editing 3D scene representation. Most methods utilize SAM [80] to produce semantic masks of input multi-view images [90, 91, 103–106], or extract dense language features, CLIP [101]/DINO [102], of each pixel [107–109].

LEGaussians [107] adds an uncertainty value attribute and semantic feature vector attribute for each Gaussian. It then renders a semantic map with uncertainties from a given viewpoint, to compare with the quantized CLIP and DINO dense features of the ground truth image. To achieve the 2D mask consistency across views, Gaussian Grouping [90] employs DEVA to propagate and associate masks from different viewpoints. It adds Identity Encoding attributes to 3D Gaussians and renders the identity feature map to compare with the extracted 2D masks.

4.2 Geometry Reconstruction and SLAM

Geometry reconstruction and SLAM are important subtasks in 3D reconstruction.

Geometry reconstruction In the context of NeRF, a series of works [110–113] have successfully reconstructed high-quality geometry from multi-view images. However, due to the discrete nature of 3DGS, only a few works stepped into this field. SuGaR [20] is the pioneering work that builds up 3D surfaces from multi-view images with the 3DGS representation. It introduces a simple but effective self-regularization loss to constrain that the distance between the camera and the closest Gaussian should be as close as possible to the corresponding pixel's depth value in the rendered depth map, which encourages the alignment between 3DGS and the authentic 3D surface. Another work NeuSG [114] chooses to incorporate the previous NeRF-based surface reconstruction method NeuS [110] in the 3DGS representation to transfer the surface property to 3DGS. More specifically,

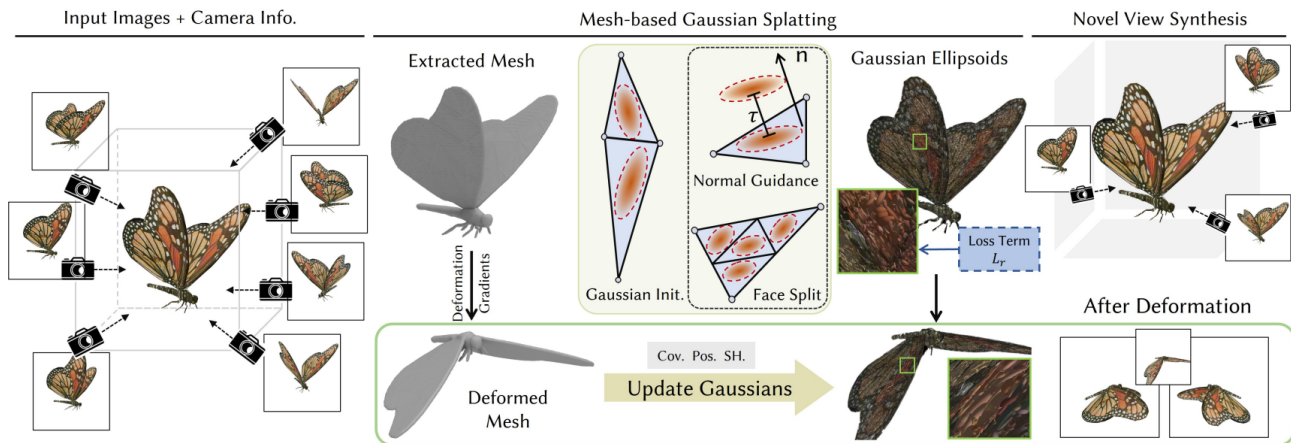


Fig. 7 Pipeline of Gao *et al.* [29]. It allows large-scale geometry editing by binding 3D Gaussians onto the mesh.

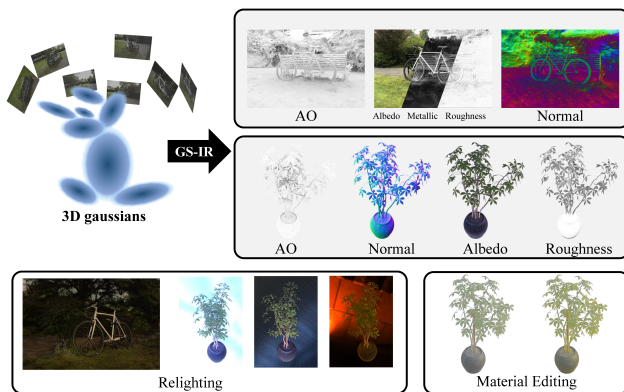


Fig. 8 By decomposing material and lighting, GS-IR [95] enables appearance editing including relighting and material manipulation.

it encourages Gaussians' signed distance values to be zeros and the normal directions of 3DGS and the NeuS method to be as consistent as possible.

SLAM There are also 3DGS methods targeting simultaneously localizing the cameras and reconstructing the 3D scenes. GS-SLAM [115] proposes an adaptive 3D Gaussian expanding strategy to add new 3D Gaussians into the training stage and delete unreliable ones with captured depths and rendered opacity values. To avoid duplicate densification, SplaTAM [116] uses view-independent colors for Gaussians and creates a densification mask to determine whether a pixel in a new frame needs densification by considering current Gaussians and the captured depth of the new frame. For stabilizing the localization and mapping, GaussianSplattingSLAM [117] and Gaussian-SLAM [118] put an extra scale regularization loss on the scale of Gaussians to encourage isotropic Gaussians. For easier initialization, LIV-GaussMap [119] initializes Gaussians with LiDAR point cloud and builds up an optimizable size-adaptive voxel

Table 4 Quantitative comparison of novel view synthesis results by different SLAM methods on the Replica [121] dataset using PSNR, SSIM and LPIPS metrics.

Methods	PSNR \uparrow	SSIM \uparrow	LPIPS \downarrow
NICE-SLAM [122]	24.42	0.81	0.23
Vox-Fusion [123]	24.41	0.80	0.24
Co-SLAM [124]	30.24	0.94	0.25
GS-SLAM [115]	31.56	0.97	0.094
SplaTAM [116]	34.11	0.97	0.10
GaussianSplattingSLAM [117]	37.50	0.96	0.07
Gaussian-SLAM [118]	38.90	0.99	0.07
SGS-SLAM [120]	34.15	0.97	0.096

grid for the global map. SGS-SLAM [120] further considers Gaussian's semantic information in the simultaneous localization and mapping process by distilling 2D semantic information which can be obtained using 2D segmentation methods or provided by the dataset. We report quantitative results by different SLAM methods on the reconstruction task in Table. 4. The explicit geometry representation provided by 3DGS enables flexible reprojection to alleviate the misalignment between different viewpoints, thus leading to better reconstruction compared to NeRF-based methods.

4.3 Digital Human

Learning virtual humans with implicit representation has been explored in various ways, especially for the NeRF and SDF representations, which exhibit high-quality results from multi-view images but suffer from heavy computational costs. Thanks to the high efficiency of 3DGS, research works have flourished and pushed 3DGS into digital human creation.

Human body In full-body modeling, works aim to reconstruct dynamic humans from multi-view videos. D3GA [125] first creates animatable human avatars using drivable 3D

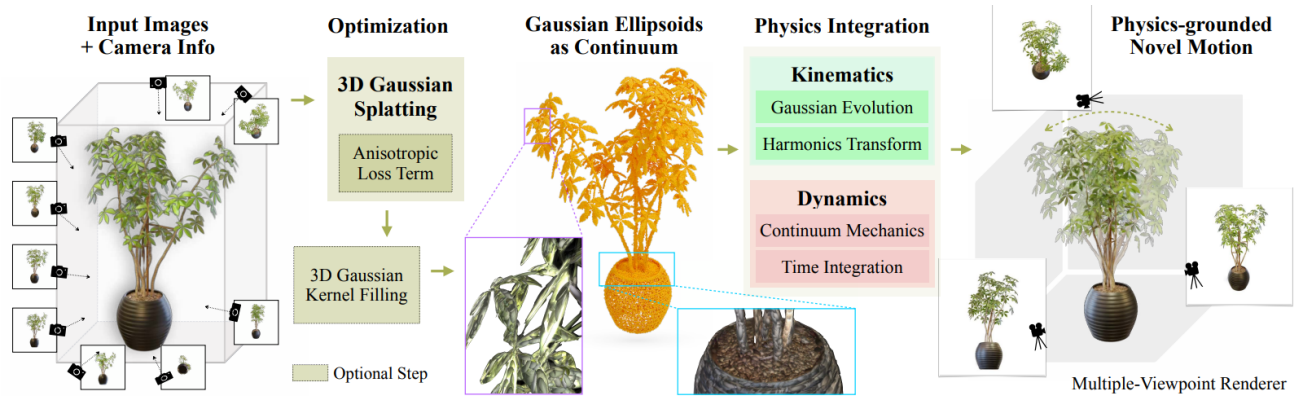


Fig. 9 Pipeline of PhysGaussian [19]. Treating 3D Gaussians as continuum, PhysGaussian [19] produces realistic physical simulation results.

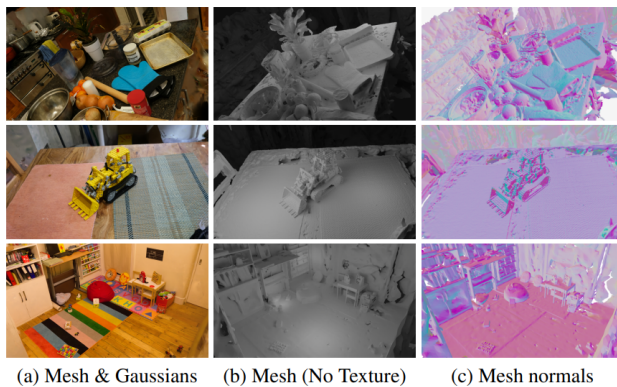


Fig. 10 Geometry reconstruction results by SuGaR [20].

Gaussians and tetrahedral cages, which achieves promising geometry and appearance modeling. To capture more dynamic details, SplatArmor [126] leverages two different MLPs to predict large motions built upon the SMPL and canonical space and allows the pose-dependent effects by the proposed $SE(3)$ fields, enabling more detailed results. HuGS [127] creates a coarse-to-fine deformation module using linear blend skinning and local learning-based refinement for constructing and animating virtual human avatars based on 3DGS. It achieves state-of-the-art human neural rendering performance at 20 FPS. Similarly, HUGS [128] utilizes the tri-plane representation [129] to factorize the canonical space, which can reconstruct the person and scene from monocular video (50–100 frames) within 30 minutes. Since 3DGS learns a huge number of Gaussian ellipsoids, HiFi4G [130] combines 3DGS with the non-rigid tracking offered by its dual-graph mechanism for high-fidelity rendering, which successfully preserves spatial-temporal consistency in a more compact manner. To achieve higher rendering speeds with high resolution on consumer-level devices, GPS-Gaussian [23] introduces Gaussian parameter maps on the sparse source view to regress the Gaussian parameters

jointly with a depth estimation module without any fine-tuning or optimization. Other than that, GART [131] extends the human to more articulated models (*e.g.*, animals) based on the 3DGS representation.

To make full use of the information from multi-view images, Animatable Gaussians [132] incorporates 3DGS and 2D CNNs for more accurate human appearances and realistic garment dynamics using a template-guided parameterization and pose projection mechanism. Gaussian Shell Maps [133] (GSMs) combines CNN-based generators with 3DGS to recreate virtual humans with sophisticated details such as clothing and accessories. ASH [134] projects the 3D Gaussian learning into a 2D texture space using mesh UV parameterization to capture the appearance, enabling real-time and high-quality animated humans. Furthermore, for reconstructing rich details on humans, such as the cloth, 3DGS-Avatar [135] introduces a shallow MLP instead of SH to model the color of 3D Gaussians and regularizes deformation with geometry priors, providing the photorealistic rendering with pose-dependent cloth deformation and generalizes to the novel poses effectively.

For dynamic digital human modeling based on monocular video, GaussianBody [138] further leverages the physical-based priors to regularize the Gaussians in the canonical space to avoid artifacts in the dynamic cloth from monocular video. GauHuman [139] re-designs the prune/split/clone of the original 3DGS to achieve efficient optimization and incorporates pose refinement and weight fields modules for fine details learning. It achieves minute-level training and real-time rendering (166 FPS). GaussianAvatar [140] incorporates the optimizable tensor with a dynamic appearance network to capture the dynamics better, allowing the dynamic avatar reconstruction and realistic novel animation in real time. Human101 [141] further pushes the speed of



Fig. 11 The results of GPS-Gaussian [23], MonoGaussianAvatar [136], and MANUS [137]. They explore the 3DGS-based approaches on the whole body, head, and hand modeling, respectively.

high-fidelity dynamic human creation to 100 seconds using a fixed-perspective camera.

Head For human head modeling with 3DGS, MonoGaussianAvatar [136] first applies 3DGS to dynamic head reconstruction using the canonical space modeling and deformation prediction. Further, PSAvatar [142] introduces the explicit Flame face model [143] to initialize Gaussians, which can capture the high-fidelity facial geometry and even complicated volumetric objects (*e.g.* glasses). The tri-plane representation and the motion fields are used in Gaussian-Head [144] to simulate geometrically changing heads in continuous movements and render rich textures, including the skin and hair. For easier head expression controllability, GaussianAvatars [145] introduce the geometric priors (Flame parametric face model [143]) into 3DGS, which binds the Gaussians onto the explicit mesh and optimize the parameters of Gaussian ellipsoids. Rig3DGS [146] employs a learnable deformation to provide stability and generalization to novel expressions, head poses, and viewing directions to achieve controllable portraits on portable devices. In another way, HeadGas [147] attributes the 3DGS with a base of latent features that are weighted by the ex-

pression vector from 3DMMs [148], which achieves real-time animatable head reconstruction. FlashAvatar [149] further embeds a uniform 3D Gaussian field in a parametric face model and learns additional spatial offsets to capture facial details, successfully pushing the rendering speed to 300 FPS. To synthesize the high-resolution results, Gaussian Head Avatar [150] adopts the super-resolution network to achieve high-fidelity head avatar learning. Apart from these, some works extend the 3DGS into text-based head generation [151], DeepFake [152], and relighting [153].

Hair and hands Other parts of humans have also been explored, such as hair and hands. 3D-PSHR [154] combines hand geometry priors (MANO) with 3DGS, which first realizes the real-time hand reconstruction. MANUS [137] further explores the interaction between the hands and object using 3DGS. In addition, GaussianHair [155] first combines the Marschner Hair Model [156] with UE4's real-time hair rendering to create the Gaussian Hair Scattering Model. It captures complex hair geometry and appearance for fast rasterization and volumetric rendering, enabling applications including editing and relighting.

4.4 3D/4D Generation

Cross-modal image generation has achieved stunning results with the diffusion model [93]. However, due to the lack of 3D data, it is difficult to directly train a large-scale 3D generation model. The pioneering work DreamFusion [69] exploits the pre-trained 2D diffusion model and proposes the score distillation sampling (SDS) loss, which distills the 2D generative priors into 3D without requiring 3D data for training, achieving text-to-3D generation. However, the NeRF representation brings heavy rendering overhead. The optimization time for each case takes several hours and the rendering resolution is low, which leads to poor-quality results. Although some improved methods extract mesh representation from trained NeRF for fine-tuning to improve the quality [157], this way will further increase optimization time. 3DGS representation can render high-resolution images with high FPS and small memory, so it replaces NeRF as the 3D representation in some recent 3D/4D generation methods.

3D generation DreamGaussian [18] replaces the MipNeRF [38] representation in the DreamFusion [69] framework with 3DGS that uses SDS loss to optimize 3D Gaussians. The splitting process of 3DGS is very suitable for the optimization progress under the generative settings, so the efficiency advantages of 3DGS can be brought to text-to-3D generation

based on the SDS loss. To improve the final quality, this work follows the idea of Magic3D [157] which extracts the mesh from the generated 3DGS and refines the texture details by optimizing UV textures through a pixel-wise Mean Squared Error (MSE) loss. In addition to 2D SDS, GSGEN [158] introduces a 3D SDS loss based on Point-E [159], a text-to-point-cloud diffusion model, to mitigate the multi-face or Janus problem. It adopts Point-E to initialize the point cloud as the initial geometry for optimization and also refines the appearance with only the 2D image prior. GaussianDreamer [160] also combines the priors of 2D and 3D diffusion models. It utilizes Shap-E [161] to generate the initial point cloud and optimizes 3DGS using 2D SDS. However, the generated initial point cloud is relatively sparse, so noisy point growth and color perturbation are further proposed to densify it. However, even if the 3D SDS loss is introduced, the Janus problem may still exist during optimization as the view is sampled one by one. Some methods [162, 163] fine-tune the 2D diffusion model [93] to generate multi-view images at once, thereby achieving multi-view supervision during SDS optimization. Or, the multi-view SDS proposed by BoostDream [164] directly creates a large 2×2 images by stitching the rendered images from 4 sampled views and calculates the gradients under the condition of the multi-view normal map. This is a plug-and-play method that can first convert a 3D asset into differentiable representations including NeRF, 3DGS, and DMTet [165] through rendering supervision, and then optimize them to improve the quality of the 3D asset. Some methods have made improvements to SDS loss. LucidDreamer [166] proposes Interval Score Matching (ISM), which replaces DDPM in SDS with DDIM inversion and introduces supervisions from interval steps of the diffusion process to avoid high error in one-step reconstruction. Some generation results are shown in Fig. 12. GaussianDiffusion [167] proposes to incorporate structured noises from multiple viewpoints to alleviate the Janus problem and variational 3DGS for better generation results by mitigating floaters. Yang *et al.* [168] point out that the differences between the diffusion prior and the training process of the diffusion model will impair the quality of 3D generation, so they propose iterative optimization of the 3D model and the diffusion prior. Specifically, two additional learnable parameters are introduced in the classifier-free guidance formula, one is a learnable unconditional embedding, and the other is additional parameters added to the network, such as LoRA [169] parameters. These methods are not limited to 3DGS, and other originally NeRF-based methods including VSD [170], CSD [171] aiming at improving the SDS loss



Fig. 12 The text-to-3D generation results of Lucidreamer [166]. It distills generative prior from pre-trained 2D diffusion models with the proposed Interval Score Matching (ISM) objective to achieve 3D generation from the text prompt.

can be used for the 3DGS generation.

As a special category, the human body can introduce the model prior, such as SMPL [172], to assist in generation. GSMs [133] builds multi-layer shells from the SMPL template and binds 3D Gaussians on the shells. By utilizing the differentiable rendering of 3DGS and the generative adversarial network of StyleGAN2 [173], animatable 3D humans are efficiently generated. GAvatar [174] adopts a primitive-based representation [175] attached to the SMPL-X [176] and attaches 3D Gaussians to the local coordinate system of each primitive. The attribute values of 3D Gaussians are predicted by an implicit network and the opacity is converted to the signed distance field through a NeuS [110]-like method, providing geometry constraints and extracting detailed textured meshes. The generation is text-based and mainly guided by the SDS loss. HumanGaussian [177] initializes 3D Gaussians by randomly sampling points on the surface of the SMPL-X [176] template. It extends Stable Diffusion [93] to generate RGB and depth simultaneously and constructs a dual-branch SDS as the optimization guidance. It also combines the classifier score provided by the null text prompt and the negative score provided by the negative prompt to construct the negative prompt guidance to address the over-saturation issue.

The above methods focus on the generation of an individual object, while scene generation requires consideration of interactions and relationships between different objects.

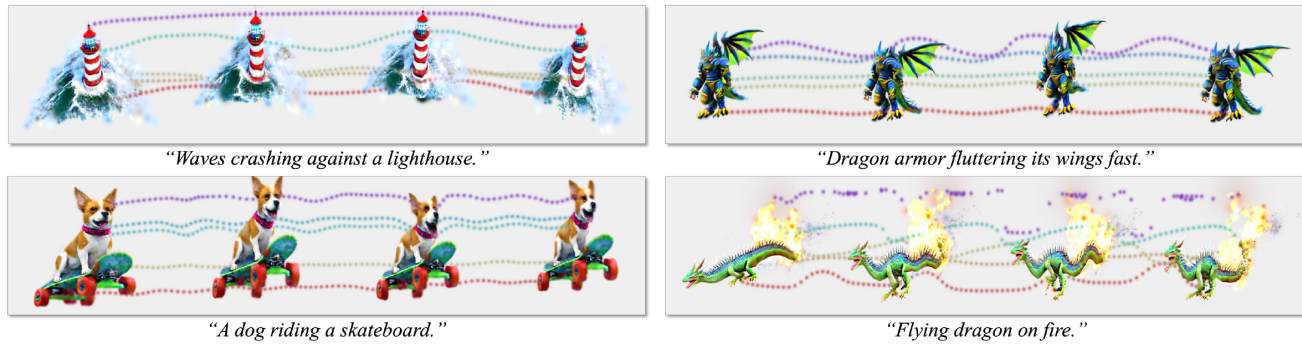


Fig. 13 The text-to-4D generation results of AYG [178]. Different dynamic 4D sequences are shown with dotted lines representing the dynamics of the deformation field.

CG3D [179] inputs a text prompt manually deconstructed by the user into a scene graph, and the textual scene graph is interpreted as a probabilistic graphical model where the directed edge has a tail of the object node and a head of the interaction node. Then scene generation becomes an ancestor sampling by first generating the objects and then their interactions. The optimization is divided into two stages, where gravity and normal contact forces are introduced in the second stage. LucidDreamer [180] and Text2Immersion [181] are both based on a reference image (user-specified or text-generated) and extend outward to achieve 3D scene generation. The former utilizes Stable Diffusion (SD) [93] for image inpainting to generate unseen regions on the sampled views and incorporates monocular depth estimation and alignment to establish a 3D point cloud from these views. Finally, the point cloud is used as the initial value, and a 3DGS is trained using the projected images as the ground truth to achieve 3D scene generation. The latter method has a similar idea, while there is a process to remove outliers in the point cloud and the 3DGS optimization has two stages: training coarse 3DGS and refinement.

Text-to-3D generation methods can be applied to image-to-3D generation, or monocular 3D reconstruction, with some simple modifications. For example, the pre-trained diffusion model used in SDS loss can be replaced with Zero-1-to-3 XL [182] for image condition [18]. We can also add losses between the input image and the corresponding rendered image under the input view to make the generation more consistent with the input image. Based on the image-to-3D generation of DreamGaussian [18], Repaint123 [183] proposes a progressive controllable repainting mechanism to refine the generated mesh texture. During the process of repainting the occlusions, it incorporates textural information from the reference image through attention feature injection [184] and proposes a visibility-aware repainting process to refine the overlap regions with different strengths. Finally, the refined

images will be used as ground truths to directly optimize the texture through MSE loss, achieving fast optimization. Other methods explore utilizing existing 3D datasets [185, 186] and constructing large models to directly generate 3DGS representation from a single image. TriplaneGaussian [24] proposes a hybrid representation of tri-plane and 3DGS. It generates a point cloud and a tri-plane encoding 3DGS's attributes information from the input image features through a transformer-based point cloud decoder and a tri-plane decoder, respectively. The generated point cloud is densified through an upsampling method and then projected onto the tri-plane to query features. The queried features are augmented by the projected image features and are translated into 3D Gaussian attributes using an MLP, thereby achieving the generation of 3DGS from a single image. AGG [187] also introduces a hybrid generator to obtain the point cloud and tri-plane features. But it first generates a coarse 3DGS and then upsamples it through a U-Net-based super-resolution module to improve the fidelity of generated results. LGM [188] first exploits the off-the-shelf models to generate multi-view images from text [162] or a single image [163]. Then it trains a U-Net-based network to generate 3DGS from the multi-view images. The U-Net is asymmetric, which allows for the input of high-resolution images while limiting the number of output Gaussians.

4D generation Based on the current progress of 3D generation, preliminary exploration has also been performed on 4D generation with 3DGS representation. AYG [178] endows 3DGS with dynamics with a deformation network for the text-to-4D generation. It is divided into two stages, static 3DGS generation with the SDS losses based on Stable Diffusion [93] and MVDream [162], and then dynamic generation with a video SDS loss based on a text-to-video diffusion model [189]. In the dynamic generation stage, only the defor-

mation field network is optimized, and some frames are randomly selected to add image-based SDS to ensure generation quality. The generation results are shown in Fig. 13. DreamGaussian4D [25] achieves 4D generation given a reference image. A static 3DGS is first generated using an improved version of DreamGaussian [18]. The off-the-shelf Stable Diffusion Video is utilized to generate a video from the given image. Then the dynamic generation is also realized by the optimization of a deformation network added to the static 3DGS, and the generated video is used as supervision, along with a 3D SDS loss based on Zero-1-to-3 XL [182] from sampled views. Finally, this method also extracts a mesh sequence and optimizes the texture with an image-to-video diffusion model. Last, for video-to-4D generation, 4DGen [190] and Efficient4D [191] both propose utilizing SyncDreamer [192] to generate multi-view images from the input frames as pseudo ground truth to train a dynamic 3DGS. The former introduces HexPlane [50] as the dynamic representation and constructs point clouds using generated multi-view images as 3D deformation pseudo ground truth. The latter directly converts 3D Gaussian into 4D Gaussian and enhances the temporal continuity of SyncDreamer [192] by fusing spatial volumes at adjacent timestamps, achieving time synchronization to generate better cross-time multi-view images for supervision.

5 Conclusions and Discussions

This survey presents an overview of the recent 3D Gaussian Splatting (3DGS) technique, which not only illustrates how it originates from traditional point-based rendering methods but also how its fast rendering and explicit geometry of the 3DGS representation facilitate a series of works targeting applications like 3D reconstruction and 3D editing. Although 3DGS has greatly improved the efficiency and results' quality on different tasks, there remain challenges for the 3D Gaussian Splatting, which can be improved by future research.

Robust novel view synthesis Although 3D Gaussian Splatting has achieved realistic novel view synthesis results, its reconstruction quality degrades as indicated by [35] when dealing with challenging inputs like sparse-view inputs, complex shading effects, and large-scale scenes. Though attempts [22, 68, 79] have been made to get better results, there are still improvement spaces. How to improve its reconstruction robustness on different inputs is an important problem.

Geometry reconstruction. Despite the efforts on the rendering quality side, few methods [20, 114] work on geom-

etry/surface reconstruction with the 3DGS representation. Compared to the continuous implicit representations like NeRF and SDF, 3DGS's geometry quality still suffers from its discrete geometry representation. Building up high-quality geometry/surface with the 3D Gaussian Splatting representation would facilitate downstream applications like automated vehicles and animations.

Independent and efficient 3D editing A few methods have dived into the field of editing 3D Gaussian Splatting's geometry [20, 26, 28, 29], texture [89, 92], and lighting [21, 22, 95, 96]. However, they cannot decompose geometry, texture, and lighting accurately or need re-optimization of Gaussians' attributes. As a result, these methods still miss independent editing capabilities or lack efficiency in the editing process. It is promising to extract geometry, texture, and lighting with more advanced rendering techniques to facilitate independent editing and build the connection between 3DGS and mesh-based representation to enable efficient editing.

Realistic 4D generation With the help of SDS loss based on SD [93], generative models [18, 24, 188] with the 3DGS representation have produced faithful results. However, 4D generation results by current methods [25, 189, 190] still miss realistic geometry, appearance, and physics-aware motion. Integrating data prior like results produced by video generative models and physical laws might boost the quality of generated 4D content.

Platform. Most implementation of methods based on the 3D Gaussian Splatting representation is written in Python with the cuda-supported PyTorch [193] framework, which may limit its future applicability on wider platforms. Reproducing it with deep learning frameworks like TensorFlow [194] and Jittor [195] can facilitate its usage on other hardware.

Declarations

Availability of data and materials As the paper does not involve the generation or analysis of specific datasets, there are no associated data or materials.

Competing interests The authors have no competing interests to declare that are relevant to the content of this article.

Funding This work was supported by National Natural Science Foundation of China (No. 62322210), Beijing Municipal Natural Science Foundation for Distinguished Young Scholars (No. JQ21013), and Beijing Municipal Science and Technology Commission (No. Z231100005923031).

Authors' contributions Tong Wu conducted an extensive literature review and drafted the manuscript. Yu-Jie Yuan, Ling-Xiao Zhang, and Jie-Yang provided critical insights, analysis of the existing research, and part of the manuscript writing. Yan-Pei Cao, Ling-Qi Yan, and Lin Gao conceived the idea and scope of the survey and improved the writing. All authors read and approved the final manuscript.

Acknowledgements We would like to thank Jia-Mu Sun and Shu-Yu Chen for their suggestion in the timeline figure.

References

- [1] Mildenhall B, Srinivasan PP, Tancik M, Barron JT, Ramamoorthi R, Ng R. NeRF: Representing Scenes as Neural Radiance Fields for View Synthesis. In *ECCV*, volume 12346, 2020, 405–421.
- [2] Müller T, Evans A, Schied C, Keller A. Instant neural graphics primitives with a multiresolution hash encoding. *ACM Trans. Graph.*, 2022, 41(4): 102:1–102:15.
- [3] Chen Z, Funkhouser TA, Hedman P, Tagliasacchi A. MobileNeRF: Exploiting the Polygon Rasterization Pipeline for Efficient Neural Field Rendering on Mobile Architectures. In *CVPR*, 2023, 16569–16578.
- [4] Yariv L, Hedman P, Reiser C, Verbin D, Srinivasan PP, Szeliski R, Barron JT, Mildenhall B. BakedSDF: Meshing Neural SDFs for Real-Time View Synthesis. In *ACM SIGGRAPH 2023 Conference Proceedings, SIGGRAPH 2023*, 2023, 46:1–46:9.
- [5] Kerbl B, Kopanas G, Leimkühler T, Drettakis G. 3D Gaussian Splatting for Real-Time Radiance Field Rendering. *ACM Trans. Graph.*, 2023, 42(4): 139:1–139:14.
- [6] Grossman JP, Dally WJ. Point Sample Rendering. In *Rendering Techniques '98, Proceedings of the Eurographics Workshop*, Eurographics, 1998, 181–192.
- [7] Zwicker M, Pfister H, van Baar J, Gross MH. Surface splatting. In *Proceedings of the 28th Annual Conference on Computer Graphics and Interactive Techniques, SIGGRAPH*, 2001, 371–378.
- [8] Zwicker M, Pfister H, van Baar J, Gross MH. EWA Volume Splatting. In *12th IEEE Visualization Conference, IEEE Vis*, 2001, 29–36.
- [9] Botsch M, Wiratanaya A, Kobbelt L. Efficient High Quality Rendering of Point Sampled Geometry. In *Eurographics Workshop on Rendering Techniques*, volume 28 of *ACM International Conference Proceeding Series*, 2002, 53–64.
- [10] Botsch M, Kobbelt L. High-Quality Point-Based Rendering on Modern GPUs. In *Pacific Conference on Computer Graphics and Applications, PG*, 2003, 335.
- [11] Rusinkiewicz S, Levoy M. QSplat: a multiresolution point rendering system for large meshes. In *Proceedings of the 27th Annual Conference on Computer Graphics and Interactive Techniques, SIGGRAPH*, 2000, 343–352.
- [12] Kobbelt L, Botsch M. A survey of point-based techniques in computer graphics. *Comput. Graph.*, 2004, 28(6): 801–814.
- [13] Chen Z, Zhang H. Learning implicit fields for generative shape modeling. In *CVPR*, 2019, 5939–5948.
- [14] Park JJ, Florence P, Straub J, Newcombe R, Lovegrove S. DeepSDF: Learning continuous signed distance functions for shape representation. In *CVPR*, 2019, 165–174.
- [15] Mescheder L, Oechsle M, Niemeyer M, Nowozin S, Geiger A. Occupancy networks: Learning 3d reconstruction in function space. In *CVPR*, 2019, 4460–4470.
- [16] Luiten J, Kopanas G, Leibe B, Ramanan D. Dynamic 3d gaussians: Tracking by persistent dynamic view synthesis. *arXiv preprint arXiv:2308.09713*, 2023.
- [17] Yang Z, Gao X, Zhou W, Jiao S, Zhang Y, Jin X. Deformable 3d gaussians for high-fidelity monocular dynamic scene reconstruction. *arXiv preprint arXiv:2309.13101*, 2023.
- [18] Tang J, Ren J, Zhou H, Liu Z, Zeng G. Dreamgaussian: Generative gaussian splatting for efficient 3d content creation. *arXiv preprint arXiv:2309.16653*, 2023.
- [19] Xie T, Zong Z, Qiu Y, Li X, Feng Y, Yang Y, Jiang C. Physgaussian: Physics-integrated 3d gaussians for generative dynamics. *arXiv preprint arXiv:2311.12198*, 2023.
- [20] Guédon A, Lepetit V. SuGaR: Surface-Aligned Gaussian Splatting for Efficient 3D Mesh Reconstruction and High-Quality Mesh Rendering. *CoRR*, 2023, abs/2311.12775.
- [21] Gao J, Gu C, Lin Y, Zhu H, Cao X, Zhang L, Yao Y. Relightable 3D Gaussian: Real-time Point Cloud Relighting with BRDF Decomposition and Ray Tracing. *CoRR*, 2023, abs/2311.16043.
- [22] Jiang Y, Tu J, Liu Y, Gao X, Long X, Wang W, Ma Y. GaussianShader: 3D Gaussian Splatting with Shading Functions for Reflective Surfaces. *CoRR*, 2023, abs/2311.17977.
- [23] Zheng S, Zhou B, Shao R, Liu B, Zhang S, Nie L, Liu Y. Gps-gaussian: Generalizable pixel-wise 3d gaussian splatting for real-time human novel view synthesis. *arXiv preprint arXiv:2312.02155*, 2023.
- [24] Zou ZX, Yu Z, Guo YC, Li Y, Liang D, Cao YP, Zhang SH. Triplane meets gaussian splatting: Fast and generalizable single-view 3d reconstruction with transformers. *arXiv preprint arXiv:2312.09147*, 2023.
- [25] Ren J, Pan L, Tang J, Zhang C, Cao A, Zeng G, Liu Z. Dreamgaussian4d: Generative 4d gaussian splatting. *arXiv preprint arXiv:2312.17142*, 2023.
- [26] Huang YH, Sun YT, Yang Z, Lyu X, Cao YP, Qi X. SC-GS: Sparse-Controlled Gaussian Splatting for Editable Dynamic Scenes. *arXiv preprint arXiv:2312.14937*, 2023.

- [27] Jiang Y, Yu C, Xie T, Li X, Feng Y, Wang H, Li M, Lau H, Gao F, Yang Y, et al.. VR-GS: A Physical Dynamics-Aware Interactive Gaussian Splatting System in Virtual Reality. *arXiv preprint arXiv:2401.16663*, 2024.
- [28] Waczyńska J, Borycki P, Tadeja S, Tabor J, Spurek P. GaMeS: Mesh-Based Adapting and Modification of Gaussian Splatting. *arXiv preprint arXiv:2402.01459*, 2024.
- [29] Gao L, Yang J, Zhang BT, Sun JM, Yuan YJ, Fu H, Lai YK. Mesh-based Gaussian Splatting for Real-time Large-scale Deformation. *arXiv preprint arXiv:2402.04796*, 2024.
- [30] Cheng K, Long X, Yang K, Yao Y, Yin W, Ma Y, Wang W, Chen X. GaussianPro: 3D Gaussian Splatting with Progressive Propagation. *arXiv preprint arXiv:*, 2024.
- [31] Yu Z, Chen A, Huang B, Sattler T, Geiger A. Mip-Splatting: Alias-free 3D Gaussian Splatting. *CoRR*, 2023, abs/2311.16493.
- [32] Yan Z, Low WF, Chen Y, Lee GH. Multi-Scale 3D Gaussian Splatting for Anti-Aliased Rendering. *CoRR*, 2023, abs/2311.17089.
- [33] Malarz D, Smolak W, Tabor J, Tadeja SK, Spurek P. Gaussian Splatting with NeRF-based Color and Opacity. *CoRR*, 2023, abs/2312.13729.
- [34] Lu T, Yu M, Xu L, Xiangli Y, Wang L, Lin D, Dai B. Scaffold-GS: Structured 3D Gaussians for View-Adaptive Rendering. *CoRR*, 2023, abs/2312.00109.
- [35] Radl L, Steiner M, Parger M, Weinrauch A, Kerbl B, Steinberger M. StopThePop: Sorted Gaussian Splatting for View-Consistent Real-time Rendering. *CoRR*, 2024, abs/2402.00525.
- [36] Yang Z, Gao X, Sun Y, Huang Y, Lyu X, Zhou W, Jiao S, Qi X, Jin X. Spec-Gaussian: Anisotropic View-Dependent Appearance for 3D Gaussian Splatting, 2024.
- [37] Barron JT, Mildenhall B, Verbin D, Srinivasan PP, Hedman P. Mip-NeRF 360: Unbounded Anti-Aliased Neural Radiance Fields. *CVPR*, 2022.
- [38] Barron JT, Mildenhall B, Tancik M, Hedman P, Martin-Brualla R, Srinivasan PP. Mip-nerf: A multiscale representation for anti-aliasing neural radiance fields. In *Proceedings of the IEEE/CVF International Conference on Computer Vision*, 2021, 5855–5864.
- [39] Barron JT, Mildenhall B, Verbin D, Srinivasan PP, Hedman P. Zip-NeRF: Anti-Aliased Grid-Based Neural Radiance Fields. *ICCV*, 2023.
- [40] Lee JC, Rho D, Sun X, Ko JH, Park E. Compact 3D Gaussian Representation for Radiance Field. *arXiv preprint arXiv:2311.13681*, 2023.
- [41] Navaneet K, Meibodi KP, Koohpayegani SA, Pirsiavash H. Compact3D: Compressing Gaussian Splat Radiance Field Models with Vector Quantization. *arXiv preprint arXiv:2311.18159*, 2023.
- [42] Niedermayr S, Stumpfegger J, Westermann R. Compressed 3d gaussian splatting for accelerated novel view synthesis. *arXiv preprint arXiv:2401.02436*, 2023.
- [43] Girish S, Gupta K, Shrivastava A. EAGLES: Efficient Accelerated 3D Gaussians with Lightweight EncodingS. *arXiv preprint arXiv:2312.04564*, 2023.
- [44] Fan Z, Wang K, Wen K, Zhu Z, Xu D, Wang Z. Light-Gaussian: Unbounded 3D Gaussian Compression with 15x Reduction and 200+ FPS. *arXiv preprint arXiv:2311.17245*, 2023.
- [45] Zeghidour N, Luebs A, Omran A, Skoglund J, Tagliasacchi M. Soundstream: An end-to-end neural audio codec. *IEEE/ACM Transactions on Audio, Speech, and Language Processing*, 2021, 30: 495–507.
- [46] MPEGGroup. MPEG Point Cloud Compression - TMC13, 2022.
- [47] Morgenstern W, Barthel F, Hilsmann A, Eisert P. Compact 3D Scene Representation via Self-Organizing Gaussian Grids. *arXiv preprint arXiv:2312.13299*, 2023.
- [48] Pumarola A, Corona E, Pons-Moll G, Moreno-Noguer F. D-nerf: Neural radiance fields for dynamic scenes. In *Proceedings of the IEEE/CVF Conference on Computer Vision and Pattern Recognition*, 2021, 10318–10327.
- [49] Wu G, Yi T, Fang J, Xie L, Zhang X, Wei W, Liu W, Tian Q, Wang X. 4d gaussian splatting for real-time dynamic scene rendering. *arXiv preprint arXiv:2310.08528*, 2023.
- [50] Cao A, Johnson J. Hexplane: A fast representation for dynamic scenes. In *Proceedings of the IEEE/CVF Conference on Computer Vision and Pattern Recognition*, 2023, 130–141.
- [51] Liang Y, Khan N, Li Z, Nguyen-Phuoc T, Lanman D, Tompkin J, Xiao L. GauFR: Gaussian Deformation Fields for Real-time Dynamic Novel View Synthesis. *arXiv preprint arXiv:2312.11458*, 2023.
- [52] Katsumata K, Vo DM, Nakayama H. An Efficient 3D Gaussian Representation for Monocular/Multi-view Dynamic Scenes. *arXiv preprint arXiv:2311.12897*, 2023.
- [53] Lin Y, Dai Z, Zhu S, Yao Y. Gaussian-Flow: 4D Reconstruction with Dynamic 3D Gaussian Particle. *arXiv preprint arXiv:2312.03431*, 2023.
- [54] Li Z, Chen Z, Li Z, Xu Y. Spacetime Gaussian Feature Splatting for Real-Time Dynamic View Synthesis. *arXiv preprint arXiv:2312.16812*, 2023.
- [55] Kratimenos A, Lei J, Daniilidis K. DynMF: Neural Motion Factorization for Real-time Dynamic View Synthesis with 3D Gaussian Splatting. *arXiv preprint arXiv:2312.00112*, 2023.
- [56] Park K, Sinha U, Hedman P, Barron JT, Bouaziz S, Goldman DB, Martin-Brualla R, Seitz SM. HyperNeRF: a higher-dimensional representation for topologically varying neural radiance fields. *ACM Transactions on Graphics (TOG)*, 2021, 40(6): 1–12.
- [57] Fang J, Yi T, Wang X, Xie L, Zhang X, Liu W, Nießner M, Tian Q. Fast Dynamic Radiance Fields with Time-Aware Neural Voxels. In *SIGGRAPH Asia 2022 Conference Papers*, 2022.

- [58] Shao R, Zheng Z, Tu H, Liu B, Zhang H, Liu Y. Tensor4D: Efficient Neural 4D Decomposition for High-fidelity Dynamic Reconstruction and Rendering. In *Proceedings of the IEEE Conference on Computer Vision and Pattern Recognition*, 2023.
- [59] Fridovich-Keil S, Meanti G, Warburg FR, Recht B, Kanazawa A. K-Planes: Explicit Radiance Fields in Space, Time, and Appearance. In *CVPR*, 2023.
- [60] Yu H, Julin J, Milacski ZA, Niinuma K, Jeni LA. CoGS: Controllable Gaussian Splatting. *arXiv*, 2023.
- [61] Yang Z, Yang H, Pan Z, Zhu X, Zhang L. Real-time photorealistic dynamic scene representation and rendering with 4d gaussian splatting. *arXiv preprint arXiv:2310.10642*, 2023.
- [62] Shaw R, Song J, Moreau A, Nazarczuk M, Catley-Chandar S, Dhano H, Perez-Pellitero E. SWAGS: Sampling Windows Adaptively for Dynamic 3D Gaussian Splatting. *arXiv preprint arXiv:2312.13308*, 2023.
- [63] Maggioni M, Tanay T, Babiloni F, McDonagh S, Leonardis A. Tunable Convolutions with Parametric Multi-Loss Optimization. In *Proceedings of the IEEE/CVF Conference on Computer Vision and Pattern Recognition*, 2023, 20226–20236.
- [64] Cotton RJ, Peyton C. Dynamic Gaussian Splatting From Markerless Motion Capture Reconstruct Infants Movements. In *Proceedings of the IEEE/CVF Winter Conference on Applications of Computer Vision*, 2024, 60–68.
- [65] Chen Y, Wang H. EndoGaussians: Single View Dynamic Gaussian Splatting for Deformable Endoscopic Tissues Reconstruction. *arXiv preprint arXiv:2401.13352*, 2024.
- [66] Huang Y, Cui B, Bai L, Guo Z, Xu M, Ren H. Endo-4dgs: Distilling depth ranking for endoscopic monocular scene reconstruction with 4d gaussian splatting. *arXiv preprint arXiv:2401.16416*, 2024.
- [67] Zhu Z, Fan Z, Jiang Y, Wang Z. FSGS: Real-Time Few-shot View Synthesis using Gaussian Splatting. *CoRR*, 2023, abs/2312.00451.
- [68] Xiong H, Muttukuru S, Upadhyay R, Chari P, Kadambi A. SparseGS: Real-Time 360° Sparse View Synthesis using Gaussian Splatting. *Arxiv*, 2023.
- [69] Poole B, Jain A, Barron JT, Mildenhall B. Dreamfusion: Text-to-3d using 2d diffusion. *arXiv preprint arXiv:2209.14988*, 2022.
- [70] Yang C, Li S, Fang J, Liang R, Xie L, Zhang X, Shen W, Tian Q. GaussainObject: Just Taking Four Images to Get A High-Quality 3D Object with Gaussian Splatting. *arXiv preprint arXiv*, 2024.
- [71] Zhang L, Rao A, Agrawala M. Adding Conditional Control to Text-to-Image Diffusion Models. In *IEEE/CVF International Conference on Computer Vision, ICCV*, 2023, 3813–3824.
- [72] Charatan D, Li S, Tagliasacchi A, Sitzmann V. pixelSplat: 3D Gaussian Splats from Image Pairs for Scalable Generalizable 3D Reconstruction. *CoRR*, 2023, abs/2312.12337.
- [73] Yu A, Ye V, Tancik M, Kanazawa A. pixelNeRF: Neural Radiance Fields From One or Few Images. In *IEEE Conference on Computer Vision and Pattern Recognition, CVPR 2021, virtual, June 19-25, 2021*, 2021, 4578–4587.
- [74] Szymanowicz S, Rupprecht C, Vedaldi A. Splatter Image: Ultra-Fast Single-View 3D Reconstruction. *CoRR*, 2023, abs/2312.13150.
- [75] Ronneberger O, Fischer P, Brox T. U-Net: Convolutional Networks for Biomedical Image Segmentation. *CoRR*, 2015, abs/1505.04597.
- [76] Jain A, Tancik M, Abbeel P. Putting NeRF on a Diet: Semantically Consistent Few-Shot View Synthesis. In *2021 IEEE/CVF International Conference on Computer Vision, ICCV*, 2021, 5865–5874.
- [77] Yang J, Pavone M, Wang Y. FreeNeRF: Improving Few-Shot Neural Rendering with Free Frequency Regularization. In *IEEE/CVF Conference on Computer Vision and Pattern Recognition*, 2023, 8254–8263.
- [78] Chen Y, Gu C, Jiang J, Zhu X, Zhang L. Periodic Vibration Gaussian: Dynamic Urban Scene Reconstruction and Real-time Rendering. *CoRR*, 2023, abs/2311.18561.
- [79] Zhou X, Lin Z, Shan X, Wang Y, Sun D, Yang M. DrivingGaussian: Composite Gaussian Splatting for Surrounding Dynamic Autonomous Driving Scenes. *CoRR*, 2023, abs/2312.07920.
- [80] Kirillov A, Mintun E, Ravi N, Mao H, Rolland C, Gustafson L, Xiao T, Whitehead S, Berg AC, Lo WY, Dollár P, Girshick R. Segment Anything. *arXiv:2304.02643*, 2023.
- [81] Yan Y, Lin H, Zhou C, Wang W, Sun H, Zhan K, Lang X, Zhou X, Peng S. Street Gaussians for Modeling Dynamic Urban Scenes. *CoRR*, 2024, abs/2401.01339.
- [82] Xiong B, Li Z, Li Z. GauU-Scene: A Scene Reconstruction Benchmark on Large Scale 3D Reconstruction Dataset Using Gaussian Splatting. *CoRR*, 2024, abs/2401.14032.
- [83] Fu Y, Liu S, Kulkarni A, Kautz J, Efros AA, Wang X. COLMAP-Free 3D Gaussian Splatting. *CoRR*, 2023, abs/2312.07504.
- [84] Sun Y, Wang X, Zhang Y, Zhang J, Jiang C, Guo Y, Wang F. iComMa: Inverting 3D Gaussians Splatting for Camera Pose Estimation via Comparing and Matching. *CoRR*, 2023, abs/2312.09031.
- [85] Lee B, Lee H, Sun X, Ali U, Park E. Deblurring 3D Gaussian Splatting. *CoRR*, 2024, abs/2401.00834.
- [86] Li Y, Fu X, Zhao S, Jin R, Zhou SK. Sparse-view CT Reconstruction with 3D Gaussian Volumetric Representation. *CoRR*, 2023, abs/2312.15676.
- [87] Bai J, Huang L, Guo J, Gong W, Li Y, Guo Y. 360-GS: Layout-guided Panoramic Gaussian Splatting For Indoor Roaming. *CoRR*, 2024, abs/2402.00763.
- [88] Nguyen VM, Sandidge E, Mahendrakar T, White RT. Characterizing Satellite Geometry via Accelerated 3D Gaussian Splatting. *CoRR*, 2024, abs/2401.02588.

- [89] Chen Y, Chen Z, Zhang C, Wang F, Yang X, Wang Y, Cai Z, Yang L, Liu H, Lin G. GaussianEditor: Swift and Controllable 3D Editing with Gaussian Splatting, 2023.
- [90] Ye M, Danelljan M, Yu F, Ke L. Gaussian Grouping: Segment and Edit Anything in 3D Scenes, 2023.
- [91] Huang J, Yu H. Point'n Move: Interactive Scene Object Manipulation on Gaussian Splatting Radiance Fields, 2023.
- [92] Fang J, Wang J, Zhang X, Xie L, Tian Q. GaussianEditor: Editing 3D Gaussians Delicately with Text Instructions, 2023.
- [93] Rombach R, Blattmann A, Lorenz D, Esser P, Ommer B. High-Resolution Image Synthesis with Latent Diffusion Models. In *CVPR*, 2022, 10674–10685.
- [94] Haque A, Tancik M, Efros A, Holynski A, Kanazawa A. Instruct-NeRF2NeRF: Editing 3D Scenes with Instructions. In *Proceedings of the IEEE/CVF International Conference on Computer Vision*, 2023.
- [95] Liang Z, Zhang Q, Feng Y, Shan Y, Jia K. GS-IR: 3D Gaussian Splatting for Inverse Rendering. *CoRR*, 2023, abs/2311.16473.
- [96] Shi Y, Wu Y, Wu C, Liu X, Zhao C, Feng H, Liu J, Zhang L, Zhang J, Zhou B, Ding E, Wang J. GIR: 3D Gaussian Inverse Rendering for Relightable Scene Factorization. *Arxiv*, 2023, abs/2312.05133.
- [97] Verbin D, Hedman P, Mildenhall B, Zickler TE, Barron JT, Srinivasan PP. Ref-NeRF: Structured View-Dependent Appearance for Neural Radiance Fields. In *IEEE/CVF Conference on Computer Vision and Pattern Recognition, CVPR*, 2022, 5481–5490.
- [98] Bonet J, Wood RD. Nonlinear continuum mechanics for finite element analysis, 1997.
- [99] Feng Y, Feng X, Shang Y, Jiang Y, Yu C, Zong Z, Shao T, Wu H, Zhou K, Jiang C, et al.. Gaussian Splashing: Dynamic Fluid Synthesis with Gaussian Splatting. *arXiv preprint arXiv:2401.15318*, 2024.
- [100] Macklin M, Müller M, Chentanez N. XPBD: position-based simulation of compliant constrained dynamics. In *Proceedings of the 9th International Conference on Motion in Games*, 2016, 49–54.
- [101] Radford A, Kim JW, Hallacy C, Ramesh A, Goh G, Agarwal S, Sastry G, Askell A, Mishkin P, Clark J, et al.. Learning transferable visual models from natural language supervision. In *International conference on machine learning*, 2021, 8748–8763.
- [102] Caron M, Touvron H, Misra I, Jégou H, Mairal J, Bojanowski P, Joulin A. Emerging properties in self-supervised vision transformers. In *Proceedings of the IEEE/CVF international conference on computer vision*, 2021, 9650–9660.
- [103] Cen J, Fang J, Yang C, Xie L, Zhang X, Shen W, Tian Q. Segment Any 3D Gaussians, 2023.
- [104] Zhou S, Chang H, Jiang S, Fan Z, Zhu Z, Xu D, Chari P, You S, Wang Z, Kadambi A. Feature 3DGS: Supercharging 3D Gaussian Splatting to Enable Distilled Feature Fields, 2023.
- [105] Qin M, Li W, Zhou J, Wang H, Pfister H. LangSplat: 3D Language Gaussian Splatting, 2023.
- [106] Hu X, Wang Y, Fan L, Fan J, Peng J, Lei Z, Li Q, Zhang Z. Segment Anything in 3D Gaussians, 2024.
- [107] Shi JC, Wang M, Duan HB, Guan SH. Language Embedded 3D Gaussians for Open-Vocabulary Scene Understanding, 2023.
- [108] Zuo X, Samangouei P, Zhou Y, Di Y, Li M. FMGS: Foundation Model Embedded 3D Gaussian Splatting for Holistic 3D Scene Understanding, 2024.
- [109] Dou B, Zhang T, Ma Y, Wang Z, Yuan Z. CoSSegGaussians: Compact and Swift Scene Segmenting 3D Gaussians with Dual Feature Fusion, 2024.
- [110] Wang P, Liu L, Liu Y, Theobalt C, Komura T, Wang W. NeuS: Learning Neural Implicit Surfaces by Volume Rendering for Multi-view Reconstruction. In *Advances in Neural Information Processing Systems 34: Annual Conference on Neural Information Processing Systems*, 2021, 27171–27183.
- [111] Liu Y, Wang L, Yang J, Chen W, Meng X, Yang B, Gao L. NeUDF: Leaning Neural Unsigned Distance Fields with Volume Rendering. In *IEEE/CVF Conference on Computer Vision and Pattern Recognition, CVPR*, 2023, 237–247.
- [112] Zhuang Y, Zhang Q, Feng Y, Zhu H, Yao Y, Li X, Cao Y, Shan Y, Cao X. Anti-Aliased Neural Implicit Surfaces with Encoding Level of Detail. In *SIGGRAPH Asia 2023 Conference Papers, SA*, 2023, 119:1–119:10.
- [113] Ge W, Hu T, Zhao H, Liu S, Chen Y. Ref-NeuS: Ambiguity-Reduced Neural Implicit Surface Learning for Multi-View Reconstruction with Reflection. In *IEEE/CVF International Conference on Computer Vision, ICCV*, 2023, 4228–4237.
- [114] Chen H, Li C, Lee GH. NeuSG: Neural Implicit Surface Reconstruction with 3D Gaussian Splatting Guidance. *CoRR*, 2023, abs/2312.00846.
- [115] Yan C, Qu D, Wang D, Xu D, Wang Z, Zhao B, Li X. GS-SLAM: Dense Visual SLAM with 3D Gaussian Splatting. *CoRR*, 2023, abs/2311.11700.
- [116] Keetha NV, Karhade J, Jatavallabhula KM, Yang G, Scherer SA, Ramanan D, Luiten J. SplatAM: Splat, Track & Map 3D Gaussians for Dense RGB-D SLAM. *CoRR*, 2023, abs/2312.02126.
- [117] Matsuki H, Murai R, Kelly PHJ, Davison AJ. Gaussian Splatting SLAM. *CoRR*, 2023, abs/2312.06741.
- [118] Yugay V, Li Y, Gevers T, Oswald MR. Gaussian-SLAM: Photo-realistic Dense SLAM with Gaussian Splatting. *CoRR*, 2023, abs/2312.10070.
- [119] Hong S, He J, Zheng X, Wang H, Fang H, Liu K, Zheng C, Shen S. LIV-GaussMap: LiDAR-Inertial-Visual Fusion for Real-time 3D Radiance Field Map Rendering. *CoRR*, 2024, abs/2401.14857.
- [120] Li M, Liu S, Zhou H. SGS-SLAM: Semantic Gaussian Splatting For Neural Dense SLAM. *CoRR*, 2024, abs/2402.03246.
- [121] Straub J, Whelan T, Ma L, Chen Y, Wijmans E, Green S, Engel JJ, Mur-Artal R, Ren CY, Verma S, Clarkson A, Yan

- M, Budge B, Yan Y, Pan X, Yon J, Zou Y, Leon K, Carter N, Briaies J, Gillingham T, Mueggler E, Pesqueira L, Savva M, Batra D, Strasdat HM, Nardi RD, Goesele M, Lovegrove S, Newcombe RA. The Replica Dataset: A Digital Replica of Indoor Spaces. *CoRR*, 2019, abs/1906.05797.
- [122] Zhu Z, Peng S, Larsson V, Xu W, Bao H, Cui Z, Oswald MR, Pollefeys M. NICE-SLAM: Neural Implicit Scalable Encoding for SLAM. In *IEEE/CVF Conference on Computer Vision and Pattern Recognition, CVPR 2022, New Orleans, LA, USA, June 18-24, 2022*, 2022, 12776–12786.
- [123] Yang X, Li H, Zhai H, Ming Y, Liu Y, Zhang G. Vox-Fusion: Dense Tracking and Mapping with Voxel-based Neural Implicit Representation. In *2022 IEEE International Symposium on Mixed and Augmented Reality (ISMAR)*, 2022, 499–507.
- [124] Wang H, Wang J, Agapito L. Co-SLAM: Joint Coordinate and Sparse Parametric Encodings for Neural Real-Time SLAM. In *CVPR*, 2023.
- [125] Zielonka W, Bagautdinov T, Saito S, Zollhöfer M, Thies J, Romero J. Drivable 3d gaussian avatars. *arXiv preprint arXiv:2311.08581*, 2023.
- [126] Jena R, Iyer GS, Choudhary S, Smith B, Chaudhari P, Gee J. Splatarmor: Articulated gaussian splatting for animatable humans from monocular rgb videos. *arXiv preprint arXiv:2311.10812*, 2023.
- [127] Moreau A, Song J, Dharmo H, Shaw R, Zhou Y, Pérez-Pellitero E. Human gaussian splatting: Real-time rendering of animatable avatars. *arXiv preprint arXiv:2311.17113*, 2023.
- [128] Kocabas M, Chang JHR, Gabriel J, Tuzel O, Ranjan A. Hugs: Human gaussian splats. *arXiv preprint arXiv:2311.17910*, 2023.
- [129] Chan ER, Lin CZ, Chan MA, Nagano K, Pan B, De Mello S, Gallo O, Guibas LJ, Tremblay J, Khamis S, et al. Efficient geometry-aware 3D generative adversarial networks. In *Proceedings of the IEEE/CVF Conference on Computer Vision and Pattern Recognition*, 2022, 16123–16133.
- [130] Jiang Y, Shen Z, Wang P, Su Z, Hong Y, Zhang Y, Yu J, Xu L. Hifi4g: High-fidelity human performance rendering via compact gaussian splatting. *arXiv preprint arXiv:2312.03461*, 2023.
- [131] Lei J, Wang Y, Pavlakos G, Liu L, Daniilidis K. Gart: Gaussian articulated template models. *arXiv preprint arXiv:2311.16099*, 2023.
- [132] Li Z, Zheng Z, Wang L, Liu Y. Animatable gaussians: Learning pose-dependent gaussian maps for high-fidelity human avatar modeling. *arXiv preprint arXiv:2311.16096*, 2023.
- [133] Abdal R, Yifan W, Shi Z, Xu Y, Po R, Kuang Z, Chen Q, Yeung DY, Wetzstein G. Gaussian shell maps for efficient 3d human generation. *arXiv preprint arXiv:2311.17857*, 2023.
- [134] Pang H, Zhu H, Kortylewski A, Theobalt C, Habermann M. Ash: Animatable gaussian splats for efficient and photoreal human rendering. *arXiv preprint arXiv:2312.05941*, 2023.
- [135] Qian Z, Wang S, Mihajlovic M, Geiger A, Tang S. 3DGS-Avatar: Animatable Avatars via Deformable 3D Gaussian Splatting. *arXiv preprint arXiv:2312.09228*, 2023.
- [136] Chen Y, Wang L, Li Q, Xiao H, Zhang S, Yao H, Liu Y. Monogaussianavatar: Monocular gaussian point-based head avatar. *arXiv preprint arXiv:2312.04558*, 2023.
- [137] Pokhariya C, Shah IN, Xing A, Li Z, Chen K, Sharma A, Sridhar S. Manus: Markerless hand-object grasp capture using articulated 3d gaussians. *arXiv preprint arXiv:2312.02137*, 2023.
- [138] Li M, Yao S, Xie Z, Chen K, Jiang YG. GaussianBody: Clothed Human Reconstruction via 3d Gaussian Splatting. *arXiv preprint arXiv:2401.09720*, 2024.
- [139] Hu S, Liu Z. Gauhuman: Articulated gaussian splatting from monocular human videos. *arXiv preprint arXiv:2312.02973*, 2023.
- [140] Hu L, Zhang H, Zhang Y, Zhou B, Liu B, Zhang S, Nie L. Gaussianavatar: Towards realistic human avatar modeling from a single video via animatable 3d gaussians. *arXiv preprint arXiv:2312.02134*, 2023.
- [141] Li M, Tao J, Yang Z, Yang Y. Human101: Training 100+ fps human gaussians in 100s from 1 view. *arXiv preprint arXiv:2312.15258*, 2023.
- [142] Zhao Z, Bao Z, Li Q, Qiu G, Liu K. PSAvatar: A Point-based Morphable Shape Model for Real-Time Head Avatar Creation with 3D Gaussian Splatting. *arXiv preprint arXiv:2401.12900*, 2024.
- [143] Li T, Bolkart T, Black MJ, Li H, Romero J. Learning a model of facial shape and expression from 4D scans. *ACM Transactions on Graphics, (Proc. SIGGRAPH Asia)*, 2017, 36(6): 194:1–194:17.
- [144] Wang J, Xie JC, Li X, Xu F, Pun CM, Gao H. GaussianHead: Impressive Head Avatars with Learnable Gaussian Diffusion. *arXiv preprint arXiv:2312.01632*, 2023.
- [145] Qian S, Kirschstein T, Schoneveld L, Davoli D, Giebenhain S, Nießner M. Gaussianavatars: Photorealistic head avatars with rigged 3d gaussians. *arXiv preprint arXiv:2312.02069*, 2023.
- [146] Rivero A, Athar S, Shu Z, Samaras D. Rig3DGS: Creating Controllable Portraits from Casual Monocular Videos. *arXiv preprint arXiv:2402.03723*, 2024.
- [147] Dharmo H, Nie Y, Moreau A, Song J, Shaw R, Zhou Y, Pérez-Pellitero E. Headgas: Real-time animatable head avatars via 3d gaussian splatting. *arXiv preprint arXiv:2312.02902*, 2023.
- [148] Blanz V, Vetter T. A morphable model for the synthesis of 3D faces. In *Seminal Graphics Papers: Pushing the Boundaries, Volume 2*, 2023, 157–164.
- [149] Xiang J, Gao X, Guo Y, Zhang J. FlashAvatar: High-Fidelity Digital Avatar Rendering at 300FPS. *arXiv preprint arXiv:2312.02214*, 2023.
- [150] Xu Y, Chen B, Li Z, Zhang H, Wang L, Zheng Z, Liu Y. Gaus-

- sian head avatar: Ultra high-fidelity head avatar via dynamic gaussians. *arXiv preprint arXiv:2312.03029*, 2023.
- [151] Zhou Z, Ma F, Fan H, Yang Y. HeadStudio: Text to Animatable Head Avatars with 3D Gaussian Splatting. *arXiv preprint arXiv:2402.06149*, 2024.
- [152] Stanishevskii G, Steczkiewicz J, Szczepanik T, Tadeja S, Tabor J, Spurek P. ImplicitDeepfake: Plausible Face-Swapping through Implicit Deepfake Generation using NeRF and Gaussian Splatting. *arXiv preprint arXiv:2402.06390*, 2024.
- [153] Saito S, Schwartz G, Simon T, Li J, Nam G. Relightable Gaussian Codec Avatars. *arXiv preprint arXiv:2312.03704*, 2023.
- [154] Jiang Z, Rahmani H, Black S, Williams BM. 3D Points Splatting for Real-Time Dynamic Hand Reconstruction. *arXiv preprint arXiv:2312.13770*, 2023.
- [155] Luo H, Ouyang M, Zhao Z, Jiang S, Zhang L, Zhang Q, Yang W, Xu L, Yu J. GaussianHair: Hair Modeling and Rendering with Light-aware Gaussians. *arXiv preprint arXiv:2402.10483*, 2024.
- [156] Marschner SR, Jensen HW, Cammarano M, Worley S, Hanrahan P. Light scattering from human hair fibers. *ACM Transactions on Graphics (TOG)*, 2003, 22(3): 780–791.
- [157] Lin CH, Gao J, Tang L, Takikawa T, Zeng X, Huang X, Kreis K, Fidler S, Liu MY, Lin TY. Magic3d: High-resolution text-to-3d content creation. In *Proceedings of the IEEE/CVF Conference on Computer Vision and Pattern Recognition*, 2023, 300–309.
- [158] Chen Z, Wang F, Liu H. Text-to-3d using gaussian splatting. *arXiv preprint arXiv:2309.16585*, 2023.
- [159] Nichol A, Jun H, Dhariwal P, Mishkin P, Chen M. Point-e: A system for generating 3d point clouds from complex prompts. *arXiv preprint arXiv:2212.08751*, 2022.
- [160] Yi T, Fang J, Wu G, Xie L, Zhang X, Liu W, Tian Q, Wang X. Gaussiandreamer: Fast generation from text to 3d gaussian splatting with point cloud priors. *arXiv preprint arXiv:2310.08529*, 2023.
- [161] Jun H, Nichol A. Shap-e: Generating conditional 3d implicit functions. *arXiv preprint arXiv:2305.02463*, 2023.
- [162] Shi Y, Wang P, Ye J, Long M, Li K, Yang X. Mv-dream: Multi-view diffusion for 3d generation. *arXiv preprint arXiv:2308.16512*, 2023.
- [163] Wang P, Shi Y. ImageDream: Image-Prompt Multi-view Diffusion for 3D Generation. *ArXiv*, 2023, abs/2312.02201.
- [164] Yu Y, Zhu S, Qin H, Li H. BoostDream: Efficient Refining for High-Quality Text-to-3D Generation from Multi-View Diffusion. *arXiv preprint arXiv:2401.16764*, 2024.
- [165] Shen T, Gao J, Yin K, Liu MY, Fidler S. Deep marching tetrahedra: a hybrid representation for high-resolution 3d shape synthesis. *Advances in Neural Information Processing Systems*, 2021, 34: 6087–6101.
- [166] Liang Y, Yang X, Lin J, Li H, Xu X, Chen Y. Luciddreamer: Towards high-fidelity text-to-3d generation via interval score matching. *arXiv preprint arXiv:2311.11284*, 2023.
- [167] Li X, Wang H, Tseng KK. GaussianDiffusion: 3D Gaussian Splatting for Denoising Diffusion Probabilistic Models with Structured Noise. *arXiv preprint arXiv:2311.11221*, 2023.
- [168] Yang X, Chen Y, Chen C, Zhang C, Xu Y, Yang X, Liu F, Lin G. Learn to Optimize Denoising Scores for 3D Generation: A Unified and Improved Diffusion Prior on NeRF and 3D Gaussian Splatting. *arXiv preprint arXiv:2312.04820*, 2023.
- [169] Hu EJ, Shen Y, Wallis P, Allen-Zhu Z, Li Y, Wang S, Wang L, Chen W. Lora: Low-rank adaptation of large language models. *arXiv preprint arXiv:2106.09685*, 2021.
- [170] Wang Z, Lu C, Wang Y, Bao F, Li C, Su H, Zhu J. ProlificDreamer: High-Fidelity and Diverse Text-to-3D Generation with Variational Score Distillation. *arXiv preprint arXiv:2305.16213*, 2023.
- [171] Yu X, Guo YC, Li Y, Liang D, Zhang SH, Qi X. Text-to-3d with classifier score distillation. *arXiv preprint arXiv:2310.19415*, 2023.
- [172] Loper M, Mahmood N, Romero J, Pons-Moll G, Black MJ. SMPL: A skinned multi-person linear model. In *Seminal Graphics Papers: Pushing the Boundaries, Volume 2*, 2023, 851–866.
- [173] Karras T, Laine S, Aittala M, Hellsten J, Lehtinen J, Aila T. Analyzing and Improving the Image Quality of StyleGAN. In *Proc. CVPR*, 2020.
- [174] Yuan Y, Li X, Huang Y, De Mello S, Nagano K, Kautz J, Iqbal U. GAvatar: Animatable 3D Gaussian Avatars with Implicit Mesh Learning. *arXiv preprint arXiv:2312.11461*, 2023.
- [175] Lombardi S, Simon T, Schwartz G, Zollhoefer M, Sheikh Y, Saragih J. Mixture of volumetric primitives for efficient neural rendering. *ACM Transactions on Graphics (ToG)*, 2021, 40(4): 1–13.
- [176] Pavlakos G, Choutas V, Ghorbani N, Bolkart T, Osman AA, Tzionas D, Black MJ. Expressive body capture: 3d hands, face, and body from a single image. In *Proceedings of the IEEE/CVF conference on computer vision and pattern recognition*, 2019, 10975–10985.
- [177] Liu X, Zhan X, Tang J, Shan Y, Zeng G, Lin D, Liu X, Liu Z. Humangaussian: Text-driven 3d human generation with gaussian splatting. *arXiv preprint arXiv:2311.17061*, 2023.
- [178] Ling H, Kim SW, Torralba A, Fidler S, Kreis K. Align Your Gaussians: Text-to-4D with Dynamic 3D Gaussians and Composed Diffusion Models. *arXiv preprint*, 2023.
- [179] Vilesov A, Chari P, Kadambi A. Cg3d: Compositional generation for text-to-3d via gaussian splatting. *arXiv preprint arXiv:2311.17907*, 2023.
- [180] Chung J, Lee S, Nam H, Lee J, Lee KM. Luciddreamer: Domain-free generation of 3d gaussian splatting scenes. *arXiv preprint arXiv:2311.13384*, 2023.
- [181] Ouyang H, Heal K, Lombardi S, Sun T. Text2Immersion: Generative Immersive Scene with 3D Gaussians. *arXiv preprint arXiv:2312.09242*, 2023.
- [182] Liu R, Wu R, Van Hoorick B, Tokmakov P, Zakharov S,

- Vondrick C. Zero-1-to-3: Zero-shot one image to 3d object. In *Proceedings of the IEEE/CVF International Conference on Computer Vision*, 2023, 9298–9309.
- [183] Zhang J, Tang Z, Pang Y, Cheng X, Jin P, Wei Y, Yu W, Ning M, Yuan L. Repaint123: Fast and High-quality One Image to 3D Generation with Progressive Controllable 2D Repainting. *arXiv preprint arXiv:2312.13271*, 2023.
- [184] Cao M, Wang X, Qi Z, Shan Y, Qie X, Zheng Y. MasaCtrl: Tuning-Free Mutual Self-Attention Control for Consistent Image Synthesis and Editing. *arXiv preprint arXiv:2304.08465*, 2023.
- [185] Deitke M, Schwenk D, Salvador J, Weihs L, Michel O, VanderBilt E, Schmidt L, Ehsani K, Kembhavi A, Farhadi A. Objaverse: A universe of annotated 3d objects. In *Proceedings of the IEEE/CVF Conference on Computer Vision and Pattern Recognition*, 2023, 13142–13153.
- [186] Deitke M, Liu R, Wallingford M, Ngo H, Michel O, Kusupati A, Fan A, Laforte C, Voleti V, Gadre SY, et al.. Objaverse-xl: A universe of 10m+ 3d objects. *arXiv preprint arXiv:2307.05663*, 2023.
- [187] Xu D, Yuan Y, Mardani M, Liu S, Song J, Wang Z, Vahdat A. AGG: Amortized Generative 3D Gaussians for Single Image to 3D. *arXiv preprint arXiv:2401.04099*, 2024.
- [188] Tang J, Chen Z, Chen X, Wang T, Zeng G, Liu Z. LGM: Large Multi-View Gaussian Model for High-Resolution 3D Content Creation. *arXiv preprint arXiv:2402.05054*, 2024.
- [189] Blattmann A, Rombach R, Ling H, Dockhorn T, Kim SW, Fidler S, Kreis K. Align your latents: High-resolution video synthesis with latent diffusion models. In *Proceedings of the IEEE/CVF Conference on Computer Vision and Pattern Recognition*, 2023, 22563–22575.
- [190] Yin Y, Xu D, Wang Z, Zhao Y, Wei Y. 4dgen: Grounded 4d content generation with spatial-temporal consistency. *arXiv preprint arXiv:2312.17225*, 2023.
- [191] Pan Z, Yang Z, Zhu X, Zhang L. Fast Dynamic 3D Object Generation from a Single-view Video. *arXiv preprint arXiv:2401.08742*, 2024.
- [192] Liu Y, Lin C, Zeng Z, Long X, Liu L, Komura T, Wang W. Syncdreamer: Generating multiview-consistent images from a single-view image. *arXiv preprint arXiv:2309.03453*, 2023.
- [193] Paszke A, Gross S, Chintala S, Chanan G, Yang E, DeVito Z, Lin Z, Desmaison A, Antiga L, Lerer A. Automatic differentiation in PyTorch, 2017.
- [194] Abadi M, Barham P, Chen J, Chen Z, Davis A, Dean J, Devin M, Ghemawat S, Irving G, Isard M, Kudlur M, Levenberg J, Monga R, Moore S, Murray DG, Steiner B, Tucker PA, Vasudevan V, Warden P, Wicke M, Yu Y, Zheng X. TensorFlow: A System for Large-Scale Machine Learning. In K Keeton, T Roscoe, editors, *12th USENIX Symposium on Operating Systems Design and Implementation, OSDI*, 2016, 265–283.
- [195] Hu S, Liang D, Yang G, Yang G, Zhou W. Jittor: a novel deep

learning framework with meta-operators and unified graph execution. *Sci. China Inf. Sci.*, 2020, 63(12).

Author biography



Tong Wu received his bachelor's degree in computer science from Huazhong University of Science and Technology in 2019. He is currently a PhD candidate at the Institute of Computing Technology, Chinese Academy of Sciences. His research interests include computer graphics and computer vision.



Yu-Jie Yuan received the bachelor's degree in mathematics from Xi'an Jiaotong University in 2018. He is currently a Ph.D. candidate at the Institute of Computing Technology, Chinese Academy of Sciences. His research interests include computer graphics and neural rendering.



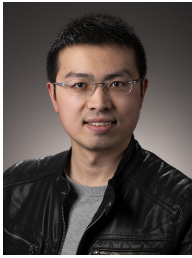
Ling-Xiao Zhang received the master of engineering's degree in computer technology from the Chinese Academy of Sciences in 2020. He is currently an engineer at the Institute of Computing Technology, Chinese Academy of Sciences. His research interests include computer graphics and geometric processing.



Jie Yang received a bachelor's degree in mathematics from Sichuan University and a Ph.D. degree in computer science from Institute of Computing Technology, Chinese Academy of Sciences. He is currently an Assistant Professor at the Institute of Computing Technology, Chinese Academy of Sciences. His research interests include computer graphics and geometric processing.



Yan-Pei Cao received bachelor's and Ph.D. degrees in computer science from Tsinghua University in 2013 and 2018, respectively. He is currently the Head of Research and Founding Team at VAST. His research interests include computer graphics and 3D computer vision.



Ling-Qi Yan is an Assistant Professor of Computer Science at UC Santa Barbara, co-director of the MIRAGE Lab, and affiliated faculty in the Four Eyes Lab. Before joining UCSB, he received his Ph.D. degree from the Department of Electrical Engineering and Computer Sciences at UC Berkeley.



Lin Gao received the bachelor's degree in mathematics from Sichuan University and the PhD degree in computer science from Tsinghua University. He is currently a Professor at the Institute of Computing Technology, Chinese Academy of Sciences. He has been awarded the Newton Advanced Fellowship from the Royal Society and the Asia Graphics

Association young researcher award. His research interests include computer graphics and geometric processing.